Supporting information

for

# Immunogenic cell death-inducing Rh(I) and Ir(I) complexes with bis(imino)acenaphthene-derived ligands: Insights into the role of the metal center and the ligands

Chengnan Wu,[1,≠], Nikolai F. Romashev,[2,≠] Veronika I. Komlyagina,[2] Tamara Petrović,[1] Ivan V. Bakaev,[2] Pavel A. Abramov,[2,3] Yuan Wang,[4] Alexey A. Ryadun,[2] Iakov S. Fomenko,[2] Taotao Zou,[4,*] Artem L. Gushchin[2,*] and Maria V. Babak[1,*]

[1] Drug Discovery Lab, Department of Chemistry, City University of Hong Kong, 83 Tat Chee Avenue, Hong Kong SAR, 999077, People's Republic of China

[2] Nikolaev Institute of Inorganic Chemistry SB RAS, 3 Acad. Lavrentiev Ave., Novosibirsk, 630090, Russian Federation

[3] Research School of Chemistry and Applied Biomedical Sciences, Tomsk Polytechnic University, Tomsk 634034, Russian Federation

[4] Guangdong Key Laboratory of Chiral Molecule and Drug Discovery, School of Pharmaceutical Sciences, Sun Yat-Sen University, Guangzhou 510006, People's Republic of China

≠ equally contributing authors

* Corresponding authors. E-mail: zoutt3@mail.sysu.edu.cn (Taotao Zou), gushchin@niic.nsc.ru (Artem L. Gushchin), mbabak@cityu.edu.hk (Maria V. Babak)

## Table of Contents

## Experimental details

**Physical Measurements.** IR spectra was recorded in the 4000-300 $cm^{-1}$ range with a Perkin-Elmer System 2000 FTIR spectrometer (KBr pellets). $^{1}H$ NMR spectra (500 MHz) were acquired on a Bruker Avance-500 spectrometer with a 5 mm PABBO-PLUS probe at room temperature. $^{1}H$ NMR stability studies were performed over the period of 72 h in DMSO-$d^6$. The chemical shifts were given in parts per million (ppm) from tetramethylsilane. Elemental C, H, N, S analysis was performed with a EuroEA3000 Eurovectoranalyzer. ESI mass spectra measurements of complexes were carried out on a high-resolution mass spectrometer (Sciex X500R Q-TOF). The cyclic voltammograms (CV) were recorded with a 797 VA Computrace system (Metrohm, Switzerland). Excitation and emission photoluminescence spectra were recorded with a Horiba Jobin Yvon Fluorolog 3 photoluminescence spectrometer equipped with 450W ozone-free Xe-lamp, cooled PC177CE-010 photon detection module with a PMT R2658 and double grating excitation and emission monochromators. Excitation and emission spectra were corrected for source intensity (lamp and grating) and emission spectral response (detector and grating) by standard correction curves. ICP-OES determination of Ir/Rh content was determined using ICP-OES Avio$^{TM}$ 220 Max spectrometer (Perkin Elmer, Watham, MA, USA). The absorbance of thiazolyl blue tetrazolium bromide (MTT) and HMGB1 ELISA kit were measured using the Multiskan Skyhigh microplate reader (Thermo Fisher scientific, USA). Flow cytometry was performed using a Cytoflex flow cytometer (Beckman Coulter, Brea, CA, USA). A Sorvall ST8R high-speed centrifuge (Thermo Fisher Scientific, USA) was utilized for the separation and isolation of samples based on their density gradients. Electrophoretic mobility shift imaging was performed using ChemiDoc Touch Imaging System (Biorad, USA). The Rh and Ir intracellular content was determined by NexION 2000 ICP Mass Spectrometer (Perkin Elmer, Watham, MA, USA).

**Single crystal X-ray diffraction studies.** Crystallographic data and refinement details are given in Table S1. Main geometrical parameters are given in Table S2. The diffraction data for **1b**, **3a/b** and **4a/b** were collected on a Bruker D8 Venture diffractometer with a CMOS PHOTON III detector and IμS 3.0 source (Mo Kα radiation, λ = 0.71073 Å) at 150 K. The φ- and ω-scan techniques were employed. Absorption correction was applied by SADABS (Bruker Apex3 software suite: Apex3, SADABS-2016/2 and SAINT, version 2018.7-2; Bruker AXS Inc.: Madison, WI, 2017). The structures were solved by SHELXT[1] and refined by full-matrix least-squares treatment against $|F|^2$ in anisotropic approximation with SHELX 2019/3[2] in ShelXle program.[3] H-atoms were refined in geometrically calculated positions. In the crystal structure of **3a** $CH_2Cl_2$ molecules of crystallization demonstrate complicated orientation disorder with low occupancies. These molecules were treated by SQUEEZE procedure[4] of PLATON program.[5] This

gives 43e per formula unit which can be assigned as one additional $CH_2Cl_2$ molecule. In the crystal structure of **4** there is a possible low-temperature phase transition between $P2_1/c$ (a = 10.8740(3), b = 21.8870(6), c = 18.0203(5), β = 102.385(1)) and $P2_1/n$ (a = 18.0210(6), b = 21.8809(7), c = 21.7523(8), β = 102.386(1)). This gives an artificial electron density around Ir atom due to non-merohedral twinning. CCDC 2431160-2431164 contain the supplementary crystallographic data for **1b**, **3a/b** and **4a/b**. These data can be obtained free of charge via http://www.ccdc.cam.ac.uk/conts/retrieving.html, or from the Cambridge Crystallographic Data Centre, 12 Union Road, Cambridge CB2 1EZ, UK; fax: (+44) 1223-336-033; or e-mail: deposit@ccdc.cam.ac.uk.

**Cyclic voltammetry.** The cyclic voltammograms (CV) were recorded with a 797 VA Computrace system (Metrohm, Switzerland). All measurements were performed with a conventional three-electrode configuration consisting of glassy carbon working and platinum auxiliary electrodes and an Ag/AgCl/KCl reference electrode. The solvent used in all experiments was dichloromethane which was deoxygenated before use. Tetra-n-butylammonium hexafluorophosphate (0.1 M solution) was used as a supporting electrolyte. The concentration of the complexes was $10^{-3}$ M. The half-wave potential ($E_{1/2}$) was calculated as the half-sum of the cathodic and anodic peak potentials. Ferrocene was used as an internal standard, the $Fc/Fc^+$ potential was 0.49 V.

**Spectroscopic studies.** The fluorescence quenching of the DNA/EtBr complex was measured at the excitation wavelength of 310 nm, and the fluorescence emission was measured at 630 nm. The measurements were performed in DMSO/$H_2O$ (4:6, v/v) solution. Salmon sperm DNA was initially mixed with EtBr at a ratio of 1:1, and complexes **3a/b** and **4a/b** were added stepwise. The ratio of drug to DNA was varied from 1:4 to 2:1. The emission was recorded at 500–800 nm. Fluorescence quenching was described by the Stern–Volmer equation: $I_0/I = 1 + K_{sv}[C]$, where $I_0$ is the initial fluorescence intensity of EtBr and DNA solution, I is fluorescence intensity of EtBr and DNA solution after the addition of the quencher, Ksv is Stern–Volmer quenching constant, and [C] is the concentration of the quencher; Ksv ($M^{-1}$) was obtained by the slope of the diagram of $I_0/I$ vs [C]. DNA-binding ability was deduced from the Scatchard equation: $r/D_f = nK - rK$, where $r = \Delta I/I_0$ and $D_f$ is the molar concentration of the free metal complex. The association binding constant K ($M^{-1}$) was obtained from the slope in the Scatchard plots $r/D_f$ vs r, and the number of binding sites per DNA (n) was given by the ratio of the intercept to the slope.

**Quantum chemical calculations.** Quantum chemical calculations were performed using the ADF2022 software package[6] (ADF: SCM, Vrije Universiteit, Theoretical Chemistry: Amsterdam, The Netherlands, http://www.scm.com). The crystal structure data for **3a/b** and **4a/b** were used as

the initial point for the geometry optimization. Calculations were made within DFT using the non-empirical PBE[7] functional in combination with empirical corrections for dispersion interactions D4(EEQ)[8] with a triple-zeta basis set of Slater-type orbitals augmented with a set of polarization functions (TZP/ADF).[9] Core electrons were frozen up to 3d orbitals for Ag and 1s orbitals for C, N, and O atoms. Scalar relativistic effects were taken into account within the ZORA approximation.[10-12] Vibrational frequencies were calculated for all optimized structures to confirm that obtained stationary points refer to minima on the corresponding potential energy surface.

**Cell lines and culture conditions.** Human cancer cell lines HCT116 (human colorectal carcinoma), MDA-MB-231 (human breast adenocarcinoma), and MRC-5 (human lung fibroblasts, non-cancerous) were obtained from ATCC. HCT116, MDA-MB-231 were cultured in DMEM containing 10% FBS and 1% of Penicillin-Streptomycin (10,000 U/mL), MRC-5 were cultured in MEM containing 10% FBS and 1% of Penicillin-Streptomycin (10,000 U/mL). Cells were grown in tissue culture flasks (75 $cm^2$ and 25 $cm^2$, SPL Life Sciences Co., Ltd., Korea). All cell lines were grown at 37 °C in a humidified atmosphere of 95% air and 5% $CO_2$ and passaged when they reached 80–90% confluency. All drug stock solutions were prepared in DMSO, and the final concentration in the medium did not exceed 1%, at which cell viability was not inhibited. The Ir/Rh concentration in the stock solutions was confirmed through inductively coupled plasma optical emission spectrometry.

**Inhibition of cell viability assay.** The cytotoxicity of compounds was determined using the MTT colorimetric test. The cells were harvested from culture flasks by trypsinization and seeded into Cellstar 96-well microculture plates at the seeding density of 6000 cells per well ($6 \times 10^4$ cells/mL). After the cells were allowed to resume exponential growth for 16 h, they were exposed to drugs at different concentrations in media for 72 h. The drugs were diluted in complete medium at the desired concentration and added to each well (100 μL) and serially diluted to other wells. After exposure for 72 h, the media was replaced with MTT in media (5 mg/mL, 100 μL/well) and incubated for additional 50 min. Subsequently, the medium was aspirated, and the purple formazan crystals formed in viable cells were dissolved in DMSO (100 μL/well). Optical densities were measured at 570 nm using the Biorad microplate reader. The quantity of viable cells was expressed in terms of treated/control (T/C) values by comparison to untreated control cells, and 50% inhibitory concentrations ($IC_{50}$) were calculated from concentration-effect curves by interpolation. Evaluation was based on means from at least three independent experiments, each comprising three replicates per concentration level.

**Intracellular accumulation and fractionation.** Cellular fractionation was performed using a commercial kit (Abcam, Cas No. ab109719). HCT116 cells were seeded into Cellstar 6-well plates

(Greiner Bio-One) at a density of $1 \times 10^6$ cells/well (2 mL per well). The cells were allowed to resume exponential growth for 16 h. Cells were harvested by trypsinization, pelleted, and washed twice with 1× PBS. Following a cell count, the pellet was resuspended in 1× Buffer A to a density of $6.6 \times 10^6$ cells/mL, and equal volumes of the suspension were transferred to new microcentrifuge tubes. One aliquot of suspension was saved as the whole-cell fraction. An equal volume of the suspension was transferred to a new microcentrifuge tube for the subsequent fractionation steps. For cytosol extraction, cell suspensions were mixed with an equal volume of Buffer B (prepared by diluting the kit's Detergent I 1:1000 in Buffer A), incubated for 7 minutes at RT, following an initial centrifugation (5,000 × g, 1 min, 4°C), the supernatant was transferred to new tubes with pellets saved on ice, and then centrifuged again at 10,000 × g for 1 min. The supernatant was clarified to yield the cytosolic fraction (C). The resulting pellets were resuspended in Buffer A. For mitochondrial extraction, these suspensions were mixed with an equal volume of Buffer C (prepared by diluting the kit's Detergent II 1:25 in Buffer A), incubated for 10 minutes at RT, following an initial centrifugation (5,000 × g, 1 min, 4°C), the supernatant was transferred to new tubes with pellets saved on ice, and then centrifuged again at 10,000 × g for 1 min. The clarified supernatant constituted the mitochondrial fraction (M). The final pellet was resuspended in Buffer A as the nuclear fraction (N). All fractions then digested by heating in 50 µl of ultrapure 60% $HNO_3$ at 110ºC for 24 h. The residue was reconstituted by adding 50 µL of ultrapure 60% HNO3 and 950 µl ultrapure $H_2O$, and then filtered. The Ir/Rh content was determined by Inductively Coupled Plasma Mass Spectrometry (ICP-MS) (NexION 2000 ICP Mass Spectrometer (Perkin Elmer, Watham, MA, USA). In was used as an internal standard. Ir and Rh were measured at m/z 193 and m/z 103, respectively. Ir/Rh standards of known concentrations (1, 5, 10, 50 ppb) were used to construct the calibration curve. The mean subcellular and whole-cell Ir/Rh concentration values with SD of three independent experiments are reported.

**ROS detection by confocal microscopy.** HCT116 cells were seeded into the confocal dish (Biosharp) at a density of $5 \times 10^5$ cells/well (1 mL per well). The cells were allowed to resume exponential growth for 16 h. The cell culture medium was aspirated and washed with PBS (2 × 1 ml). In a dimly lit setting, a solution of $H_2$DCFDA (2',7'-dichlorodihydrofluorescein diacetate) in 1× HBSS (10 µM, 1 mL) was added to each well and allowed to incubate for 10 min at 37 °C. Following this, the $H_2$DCFDA solution was aspirated and the wells were rinsed with HBSS (2 ×1 mL). Subsequently, the cells were treated with fresh colourless cell culture medium containing compounds of interest at their respective 10 × $IC_{50}$ concentrations for 2 h at 37 °C. Following the incubation period, the drug-containing medium was removed and the wells were washed with PBS (2 × 1 mL). Subsequently, the cells were treated with a culture medium containing 1 µM of ER

tracker red (ThermoFisher, Cas No. E34250) (Excitation/Emission 587⁄615 nm) or 100 nM MitoTracker Deep Red FM (Excitation/Emission 644⁄665 nm) (ThermoFisher, Cas No. M22426), 1 μg/mL of Hoechst 33342 for 30 minutes. Following this incubation, the cells were washed with PBS (2 × 1 mL). The samples were then protected from light with aluminum foil before imaging. Images were captured using Laser Confocal Scanning Microscope (Leica SPE) and analyzed using the Microscope Software Platform LAS X Life Science. Colocalization was calculated by measuring Pearson's correlation coefficient (PCC) between the Ros and ER/Mitochondria dyes.

**Electrophoretic mobility shift (EMSA) assay.** 0.5 μg of pBR322 plasmid DNA (Thermo Fisher Scientific, USA) in freshly sterile-filtrated TE buffer (10 mM Tris/HCl, 1 mM EDTA, pH 8.0) were incubated with 5 μM, 10 μM, 25 μM and 50 μM of the complexes and cisplatin for 24 h at 37 °C (30 μl). DNA samples without the addition of any test substance served as negative controls. The samples were reconstituted in 10× DNA loading buffer (Catalog number: P022-01, Vazyme) and resolved on a 1% agarose gel (Beyotime) by electrophoresis at 50 V for 2 h. The images were visualized by ChemiDoc Touch Imaging System (Biorad).

**CRT detection by flow cytometry.** HCT116 cells were seeded into Cellstar 6-well plates (Greiner Bio-One) at a density of $5 \times 10^5$ cells/well (2 ml per well). The cells were allowed to resume exponential growth for 16 h. Afterwards the cells were incubated with a fresh medium containing compounds of interest at their respective 10 × $IC_{50}$ concentrations for 24 h at 37 °C. After the treatment, the supernatant was collected in 2 mL microtubes. The wells were washed with 1 ml of PBS, trypsinized with 300 μL of trypsin at 37 °C for 5 min and combined with the corresponding supernatant. The cell suspension was then centrifuged (300 × g, 7 min), washed with PBS (2 × 1 ml), stained with propidium iodide (PI) for 10 min at RT, washed with 1 ml of PBS and centrifuged again (300 × g, 7 min). Next, cells were incubated with CRT antibody conjugated with AlexaFluor S24 488 (62304S, Cell Signaling Technology) at 4 °C overnight, washed twice with PBS, reconstituted in 500 uL of PBS and analyzed by flow cytometry using a CytoFLEX Flow Cytometer equipped with a 488 nm laser and a 638 nm laser (Beckman Coulter, Brea, CA, USA). The cells were excited by the 488 nm laser, and fluorescence emissions were detected at 525/40 nm for FITC (CRT) and at 610/20 nm for ECD (PI). The resulting dot blots were acquired from 10,000 events and the PI-negative cell population was quantified using Flowjo software (version 10.8.0, BD Biosciences, San Jose, CA, USA)

**CRT detection by confocal microscopy.** HCT116 cells were seeded into confocal dishes (Biosharp) at a density of $5 \times 10^5$ cells/dish (1 ml per dish). The cells were allowed to resume exponential growth for 16 h. Afterwards, the cells were incubated with a fresh medium containing compounds at their respective 10 × $IC_{50}$ concentrations for 24 h at 37°C. After the treatment, the

dishes were washed with 1 ml of PBS, fixed in 4% paraformaldehyde in PBS at r. t. for 20 min and washed twice with 1 mL of PBS. The dishes were then incubated with CRT antibody conjugated with Alexa Fluor 488 (1:200 in PBS, 62304S, Cell Signaling Technology) at 4°C overnight and washed twice with PBS. Then the dishes were incubated with Wheat Germ Agglutinin conjugated with Alexa Fluor 633 dye (W21404, Invitrogen) at r. t. in darkness for 30 min, washed with 1 ml of PBS, stained with propidium iodide (PI) for 10 min at r. t. in darkness and washed with 1 ml of PBS. Samples were stored in 1 ml of PBS. The confocal images were acquired by Laser Confocal Scanning Microscope (Leica SPE).

**HMGB1 detection by confocal microscopy.** HCT116 cells were seeded into confocal dishes (Biosharp) at a density of $5 \times 10^5$ cells/dish (1 mL per dish). The cells were allowed to resume exponential growth for 16 h. Afterwards, the cells were incubated with a fresh medium containing compounds at their respective $10 \times IC_{50}$ concentrations for 24 h at 37°C. After the treatment, the dishes were washed with 1 ml of PBS, fixed in 4% paraformaldehyde in PBS at r. t. for 20 min and washed twice with 1 mL of PBS. Followed by penetration with 0.3% Triton X-100（ST795, Beyotime) for 10 min at r. t., the dishes were washed twice with 2 × 1 mL of PBS. The dishes were then incubated with HMGB1 antibody (1:200 dilution in PBS, 3935, Cell Signaling Technology) at 4° C overnight and washed twice with PBS. Then they were incubated with a secondary antibody conjugated with AlexaFluor 488 (ab150081, Abcam) (1:1000 dilution in PBS) at r. t. in darkness for 2 h, washed with 1 mL of PBS, stained with propidium iodide (PI) for 10 mins at r. t. in darkness and washed with 1 mL of PBS. Samples were stored in 1 mL of PBS. The confocal images were acquired by Laser Confocal Scanning Microscope (Leica SPE).

**HMGB1 detection by ELISA.** HCT116 cells were seeded into Cellstar 6-well plates (Greiner Bio-One) at a density of $2 \times 10^6$ cells/well (2 ml per well). The cells were allowed to resume exponential growth for 16 h. Afterwards the medium was replaced with fresh medium containing compounds of interest at their respective $10 \times IC_{50}$ concentrations. After 24 h, supernatants were collected and centrifuged (15,000 × rpm, 20 min), after which the pellets were discarded. The released HMGB1 levels were quantified by ELISA using the manufacturer's protocol provided with the HMGB1 ELISA kit (UpingBio Technology Co., Ltd, China). Optical densities were measured at 450 nm using the Multiskan Skyhigh microplate reader (Thermo Fisher scientific, USA).

**RealTime-Glo extracellular ATP assay.** HCT116 cells were seeded into Cellstar 96-well plates (Greiner Bio-One) at a density of $1.8 \times 10^4$ cells/well (1 ml per well). The cells were allowed to resume exponential growth for 16 h. Afterwards the medium was replaced with fresh medium containing compounds of interest at their respective $10 \times IC_{50}$ concentrations. ATP reagent was

added according to the manufacturer's protocol (RealTime-Glo Extracellular ATP Assay Kit (Catalogue number: GA5010)). Luminescence was measured using Molecular Devices SpectraMax iD5 plate reader. Measurements were taken at 2-minute intervals to capture real-time changes in extracellular ATP release. The luminescence data was recorded for a total duration of 6 h following the treatment. Kinetic graphs were generated to visualize the time-dependent changes in ATP release. An evaluation was based on means from at least three independent experiments.

**Annexin V/PI assay.** HCT116 cells were seeded into Cellstar 6-well plates (Greiner Bio-One) at a density of $5 \times 10^5$ cells/well (1 ml per well). The cells were allowed to resume exponential growth for 16 h. The medium was removed and cells were washed with PBS (2 × 1 ml). Afterwards the cells were incubated with a fresh medium containing compounds of interest at their respective 10 × $IC_{50}$ concentrations for 24 h at 37 °C. After the treatment, the supernatant was collected in 2 ml microtubes, centrifuged (300 × g, 7 min) and the media was removed. The adherent cells were then trypsinized with 500 µL of trypsin at 37 °C for 5 min. Next, 1 ml of medium was added to neutralize trypsin and the resulting cell suspension was combined with the supernatant. The wells were washed with 200 µL of PBS, which was also combined with the supernatant. The combined solutions were centrifuged (300 × g, 7 min), and the resulting pellets were washed with PBS (2 × 1 ml) and resuspended in 200 µL of Annexin V binding buffer. The cells were stained with Annexin V-FITC for 15 min in ice protected from light, and then propidium iodide (PI) was added just before each measurement. Cell death was evaluated by flow cytometry using a CytoFLEX Flow Cytometer equipped with a 488 nm laser and a 638 nm laser (Beckman Coulter, Brea, CA, USA). The cells were excited by the 488 nm laser, and fluorescence emissions were detected at 525/40 nm for FITC (Annexin V) and at 610/20 nm for ECD (PI). The resulting dot blots were acquired from 10,000 events and quantified using Flowjo software (version 10.8.0, BD Biosciences, San Jose, CA, USA).

**Table S1.** Crystallographic data for complexes **1b, 3a/b** and **4a/b**

| Complex | 1b | 3a | 3b | 4a | 4b |
|---|---|---|---|---|---|
| **Chemical formula** | $C_{40}H_{44}Cl_5N_2Rh$ | $C_{45}H_{52}F_3N_2O_3RhS$ | $C_{41}H_{44}Cl_4F_3N_2O_3RhS$ | $C_{47}H_{56}Cl_4F_3IrN_2O_3S$ | $C_{40}H_{42}Cl_2F_3IrN_2O_3S$ |
| $M_r$ | 832.93 | 860.85 | 946.55 | 1119.99 | 950.91 |
| **Crystal system, Space group** | Triclinic, $P\bar{1}$ | Trigonal, $R3{:}H$ | Monoclinic, $P2_1/n$ | Orthorhombic, *Pnma* | Monoclinic, $P2_1/c$ |
| ***a, b, c* (Å)** | 10.3796(2), 12.3721(2), 15.3778(3) | 35.110(6), 35.110(6), 10.113(2) | 12.5271(5), 21.7058(11), 15.6480(7) | 19.7915(9), 19.4195(10), 13.2190(6) | 10.8740(3), 21.8870(6), 18.0203 (5) |
| **α, β, γ (°)** | 77.627(1), 81.572(1), 78.375(1) | 90, 90, 120 | 90, 101.154(1), 90 | 90, 90, 90 | 90, 102.385(1), 90 |
| ***V* (Å$^3$)** | 1878.28 (6) | 10796 (4) | 4174.5 (3) | 5080.6 (4) | 4189.0 (2) |
| ***Z*** | 2 | 9 | 4 | 4 | 4 |
| **μ (mm$^{-1}$)** | 0.84 | 0.45 | 0.77 | 2.93 | 3.42 |
| **Crystal size (mm)** | 0.18 × 0.15 × 0.04 | 0.17 × 0.10 × 0.07 | 0.13 × 0.11 × 0.07 | 0.25 × 0.20 × 0.07 | 0.20 × 0.20 × 0.02 |
| $T_{min}$, $T_{max}$ | 0.693, 0.747 | 0.587, 0.745 | 0.685, 0.746 | 0.584, 0.746 | 0.583, 0.746 |
| **No. of measured, independent and observed [$I > 2\sigma(I)$] reflections** | 51059, 14176, 12032 | 21048, 7824, 5819 | 31421, 9207, 6757 | 28022, 6467, 5467 | 50245, 12782, 10336 |
| $R_{int}$ | 0.035 | 0.094 | 0.063 | 0.034 | 0.043 |
| **θ values (°)** | $\theta_{max}$ = 33.2, $\theta_{min}$ = 2.0 | $\theta_{max}$ = 24.4, $\theta_{min}$ = 2.4 | $\theta_{max}$ = 27.2, $\theta_{min}$ = 1.6 | $\theta_{max}$ = 28.3, $\theta_{min}$ = 2.1 | $\theta_{max}$ = 30.5, $\theta_{min}$ = 1.9 |
| **(sin θ/λ)$_{max}$ (Å$^{-1}$)** | 0.770 | 0.582 | 0.642 | 0.667 | 0.715 |
| **Range of *h, k, l*** | $-15 \le h \le 15$, $-18 \le k \le 19$, $-23 \le l \le 23$ | $-40 \le h \le 38$, $-40 \le k \le 40$, $-11 \le l \le 11$ | $-15 \le h \le 16$, $-27 \le k \le 20$, $-20 \le l \le 20$ | $-26 \le h \le 26$, $-25 \le k \le 17$, $-15 \le l \le 17$ | $-15 \le h \le 15$, $-31 \le k \le 30$, $-19 \le l \le 25$ |
| $R[F^2 > 2\sigma(F^2)]$, $wR(F^2)$, $S$ | 0.037, 0.096, 1.09 | 0.058, 0.130, 0.96 | 0.063, 0.182, 1.09 | 0.047, 0.129, 1.07 | 0.063, 0.160, 1.16 |
| **No. of reflections, parameters, restraints** | 14176, 453, 3 | 7824, 484, 4 | 9207, 492, 1 | 6467, 344, 70 | 12782, 489, 32 |
| **H-atom treatment** | H atoms treated by a mixture of independent and constrained refinement | H-atom parameters constrained | H-atom parameters constrained | H-atom parameters constrained | H-atom parameters constrained |
| **Weighting scheme** | $w = 1/[\sigma^2(F_o^2) + (0.0466P)^2 + 0.551P]$ where $P = (F_o^2 + 2F_c^2)/3$ | $w = 1/[\sigma^2(F_o^2) + (0.0483P)^2]$ where $P = (F_o^2 + 2F_c^2)/3$ | $w = 1/[\sigma^2(F_o^2) + (0.0852P)^2 + 5.4093P]$ where $P = (F_o^2 + 2F_c^2)/3$ | $w = 1/[\sigma^2(F_o^2) + (0.0672P)^2 + 14.9376P]$ where $P = (F_o^2 + 2F_c^2)/3$ | $w = 1/[\sigma^2(F_o^2) + (0.0557P)^2 + 32.1356P]$ where $P = (F_o^2 + 2F_c^2)/3$ |
| $\Delta\rho_{max}$, $\Delta\rho_{min}$ (e Å$^{-3}$) | 1.48, -1.10 | 0.93, -0.43 | 1.15, -1.69 | 1.60, -2.08 | 6.11, -1.96 |
| **Absolute structure** | – | Flack x determined using 2092 quotients [(I+)-(I-)]/[(I+)+(I-)] (Ref. [13]) | – | – | – |
| **Absolute structure parameter** | – | 0.01(3) | – | – | – |

**Table S2.** Key bond lengths and angles observed in the molecular structures of **1b, 3a/b** and **4a/b** in comparison with the previously published complex **1a**.

| **Bond lengths (Å) and angles (°)** | **1a** [ref.[14]] | **1b** | **3a** | **3b** | **4a** | **4b** |
|---|---|---|---|---|---|---|
| CCDC number | 1885194 | 2431160 | 2431161 | 2431162 | 2431163 | 2431164 |
| M–N | 2.127 (5) | 2.124 (1) | 2.105 (7) | 2.092 (3) | 2.081 (4) | 2.082 (5) |
| (M = Rh or Ir) | 2.127 (5) | 2.131 (2) | 2.108 (7) | 2.112 (3) | 2.081 (4) | 2.091 (5) |
| M–C | 2.115 (4) | 2.109 (2) | 2.138 (10) | 2.134 (4) | 2.152 (11) | 2.132 (6) |
| (M = Rh or Ir) | 2.115 (4) | 2.117 (2) | 2.138 (10) | 2.141 (5) | 2.142 (11) | 2.125 (6) |
| | 2.142 (5) | 2.130 (3) | 2.130 (11) | 2.133 (4) | 2.156 (12) | 2.118 (7) |
| | 2.142 (5) | 2.140 (2) | 2.132 (11) | 2.146 (4) | 2.139 (11) | 2.134 (6) |
| C–C | 1.486 (3) | 1.482 (2) | 1.49(1) | 1.503(6) | 1.490(8) | 1.519(8) |
| C=N | 1.294 (3) | 1.297 (2) | 1.30(1) | 1.289(5) | 1.299(5) | 1.277(7) |
| | 1.294 (3) | 1.292 (2) | 1.28(1) | 1.280(5) | 1.299(5) | 1.277(7) |
| Rh–Cl | 2.591 (3) | 2.5935 (5) | - | - | - | - |
| N–M–N | 78.13 (5) | 78.28 (5) | 78.5 (3) | 79.5 (1) | 79.1 (1) | 78.9 (2) |

**Table S3.** Composition of the frontier molecular orbitals of complexes **3a/b** and **4a/b**.

| **Orbital** | **Fragment** | **3a** | **3b** | **4a** | **4b** |
|---|---|---|---|---|---|
| **HOMO** | Rh/Ir | 82.35 % | 85.83 % | 76.01 % | 84.31 % |
| | Ar-bian | 1.54 % | 0 % | 5.06 % | 0 % |
| **LUMO** | Rh/Ir | 1.92 % | 4.64 % | 8.29 % | 5.58 % |
| | Ar-bian | 81.01 % | 80.15 % | 77.68 % | 79.14 % |

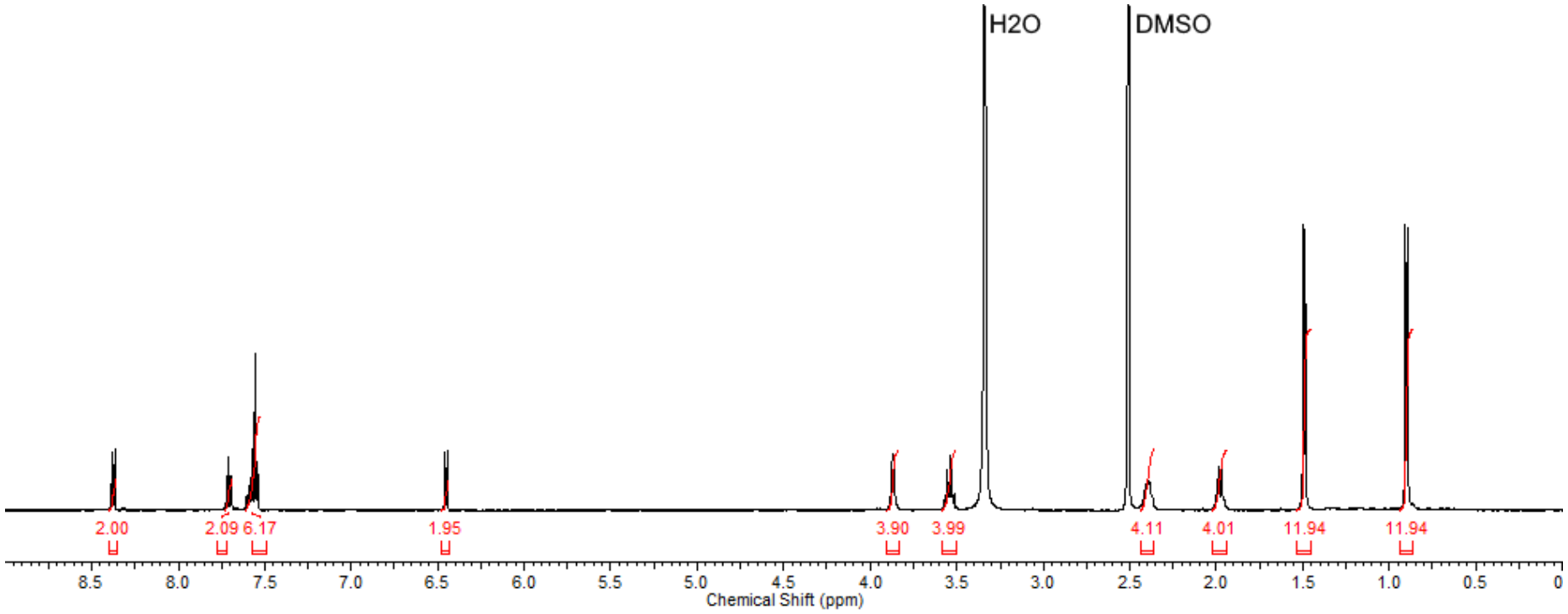


**Figure S1.** $^{1}$H NMR spectrum of **3a** in DMSO-d$^{6}$.

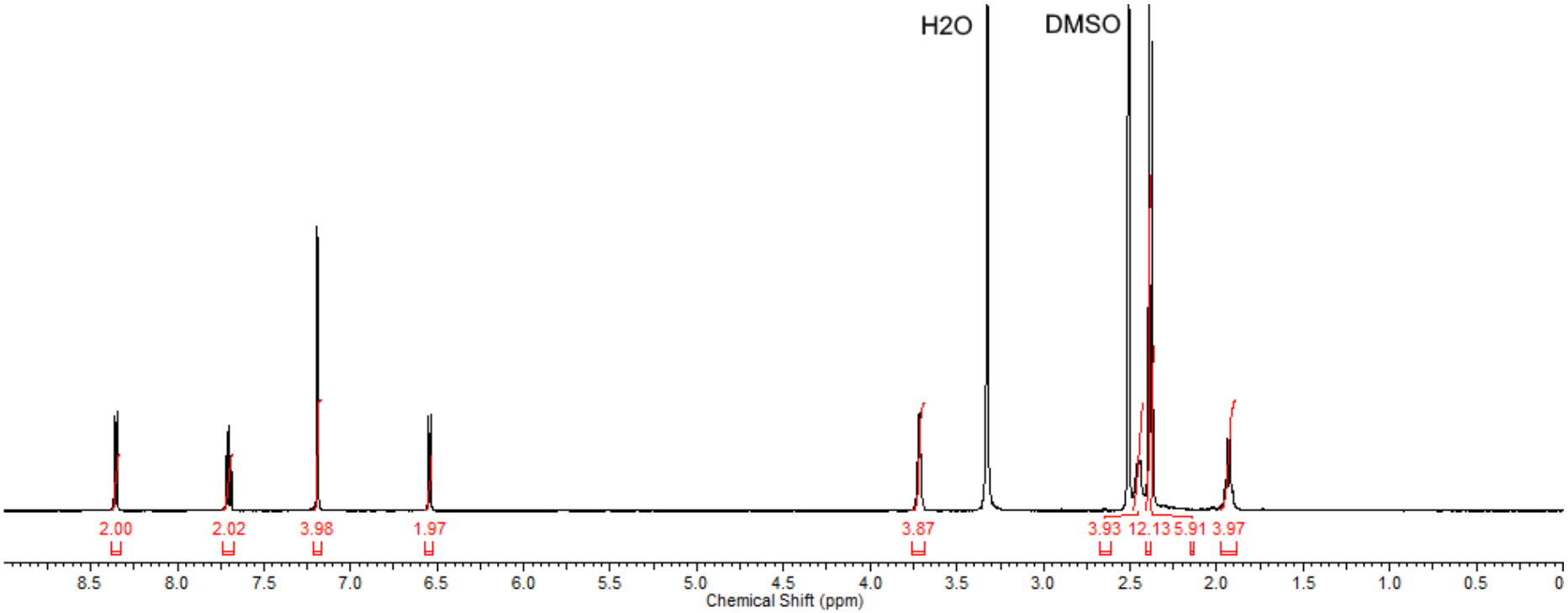


**Figure S2.** $^{1}$H NMR spectrum of **3b** in DMSO-d$^{6}$.

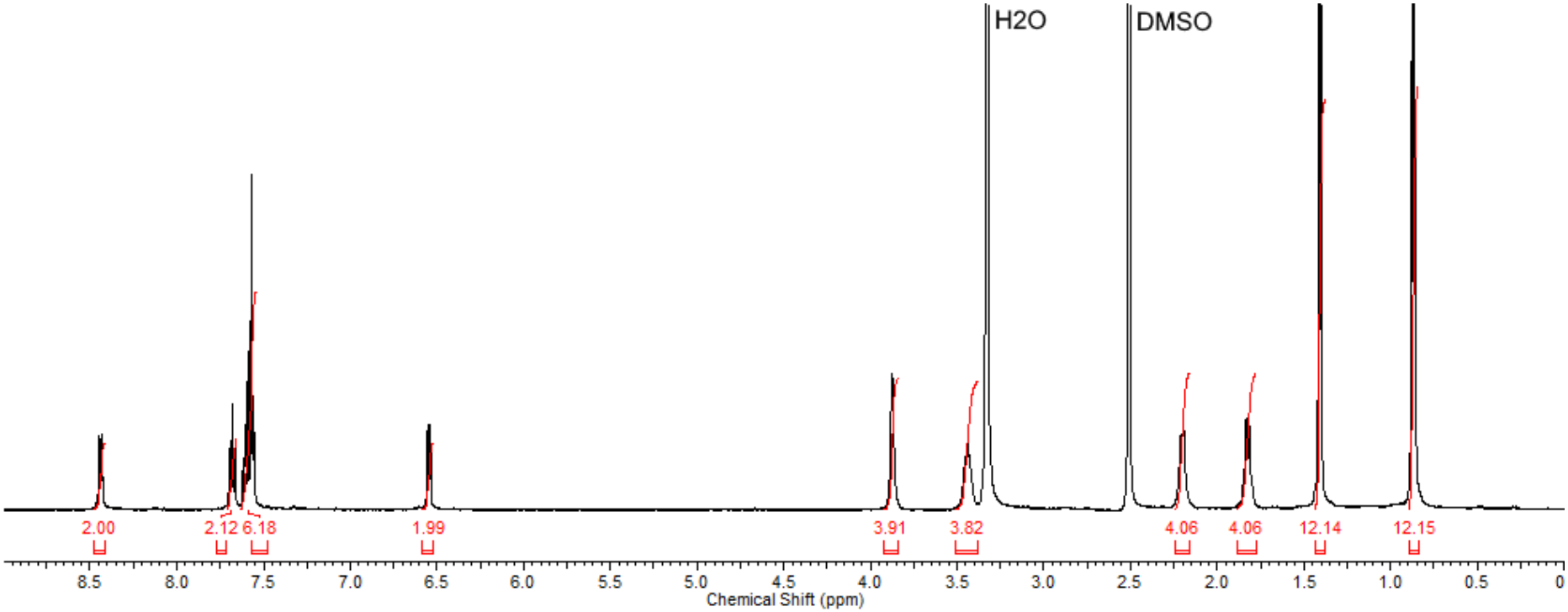


**Figure S3.** $^{1}$H NMR spectrum of **4a** in DMSO-d$^{6}$.

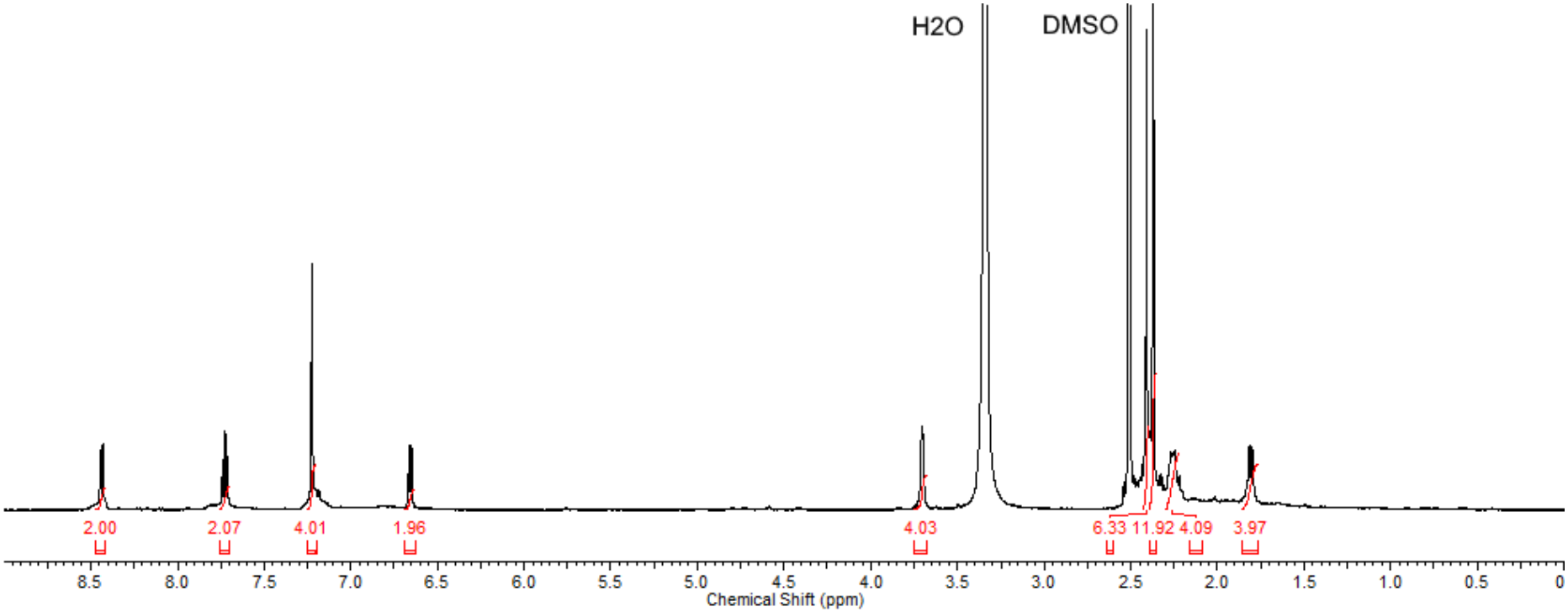


**Figure S4.** $^{1}$H NMR spectrum of **4b** in DMSO-d$^{6}$.

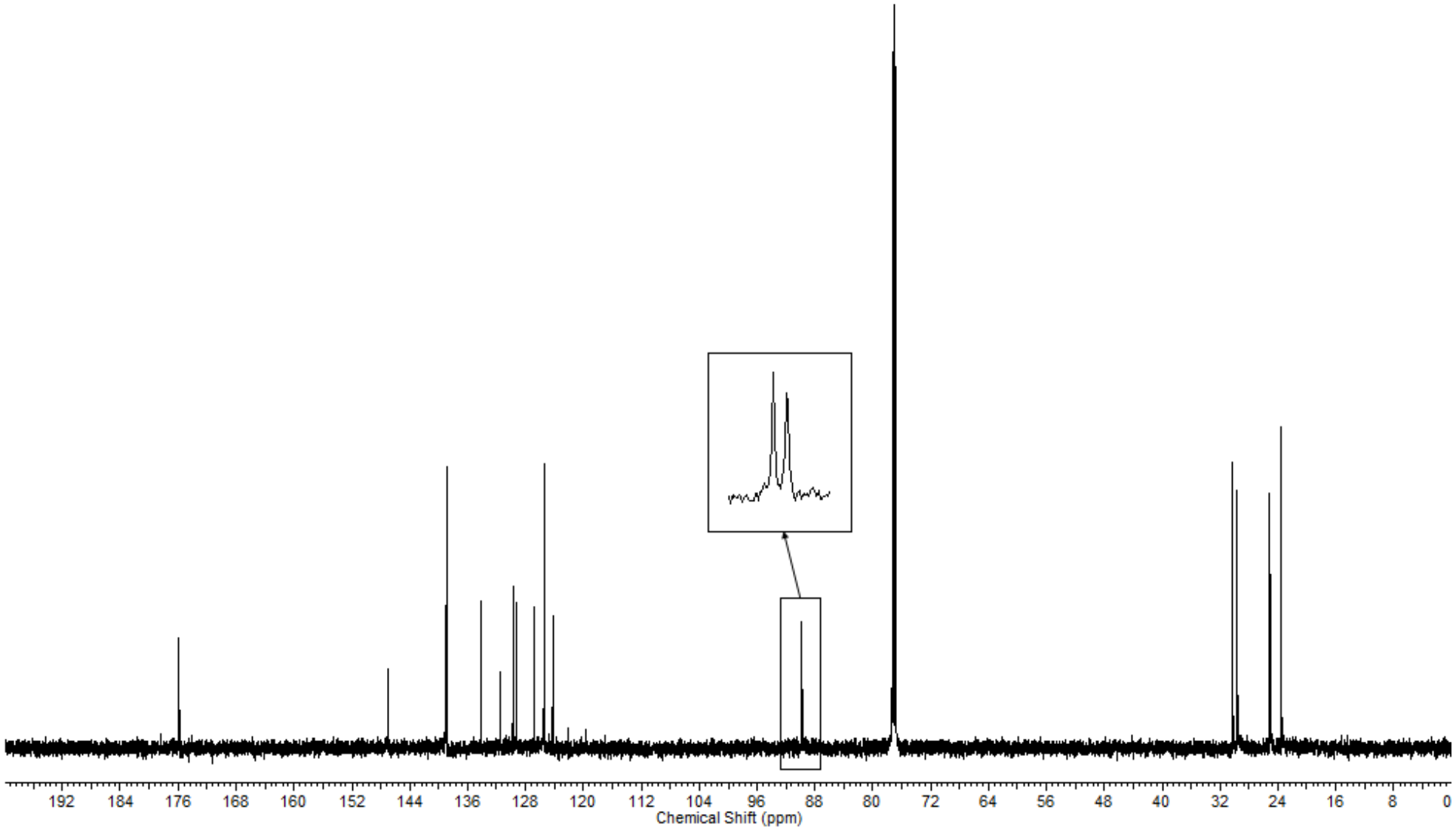


**Figure S5.** $^{13}C$ NMR spectrum of **3a** in $CDCl_3$.

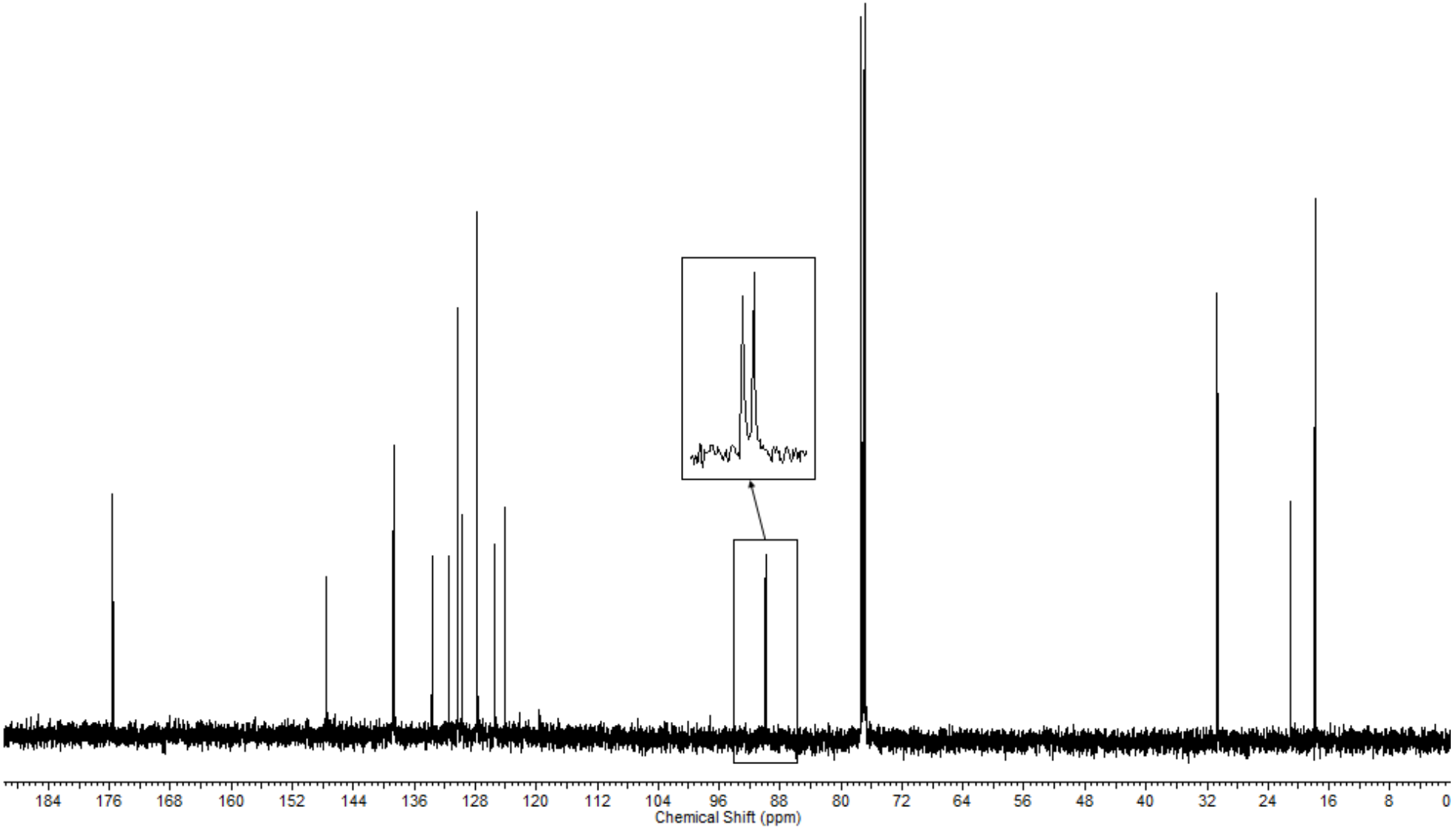


**Figure S6.** $^{13}C$ NMR spectrum of **3b** in $CDCl_3$.

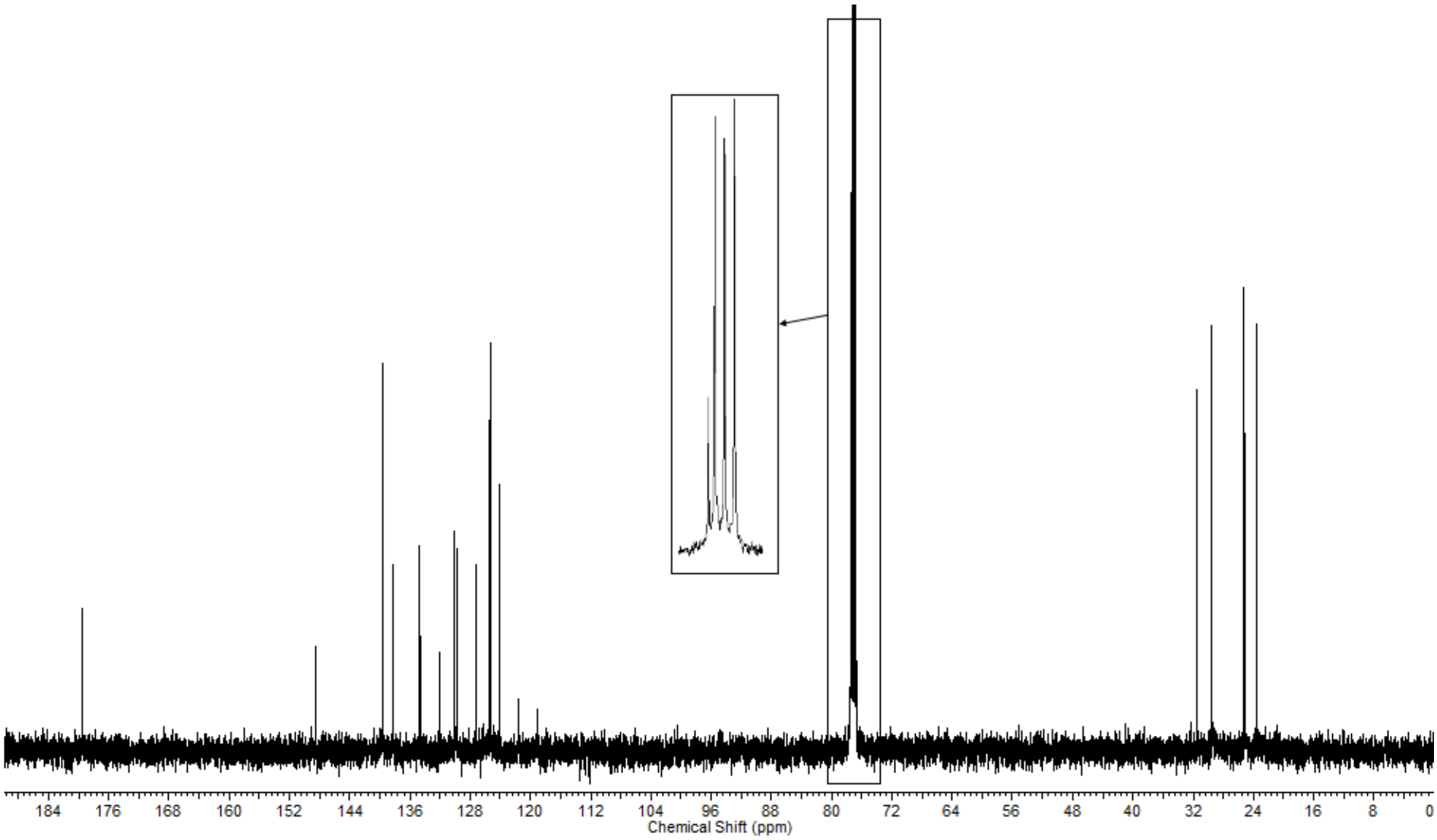


**Figure S7.** $^{13}C$ NMR spectrum of **4a** in $CDCl_3$.

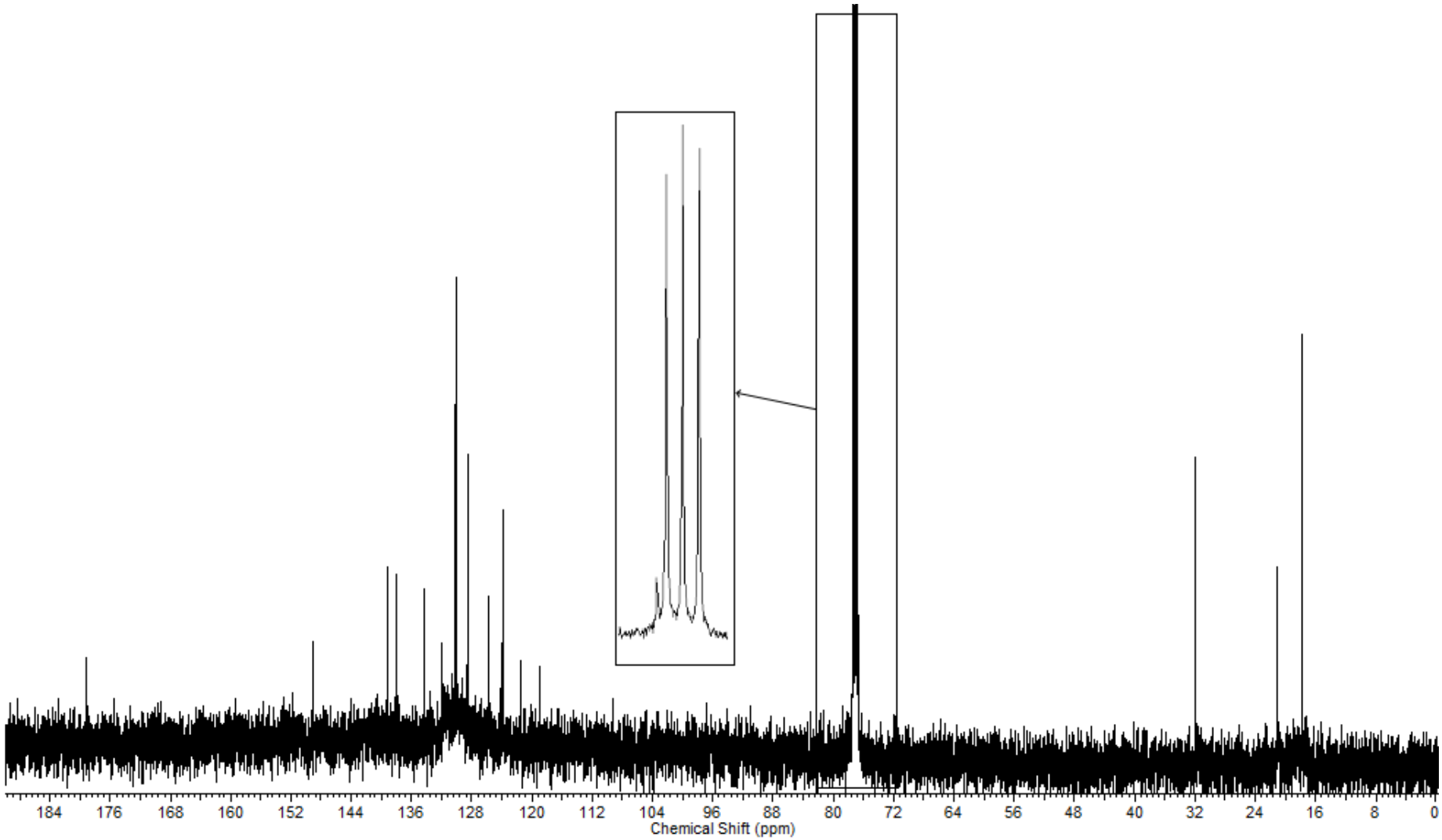


**Figure S8.** $^{13}C$ NMR spectrum of **4b** in $CDCl_3$.

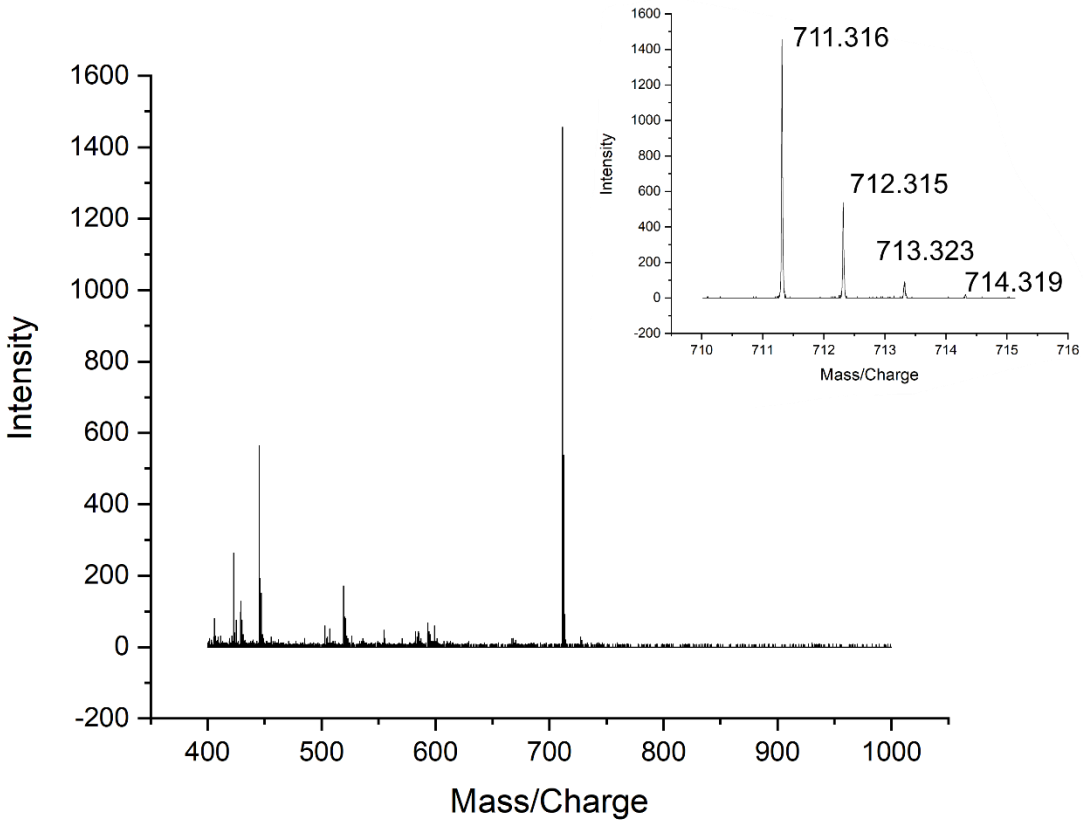


**Figure S9.** High resolution ESI-MS spectrum of **3a**.

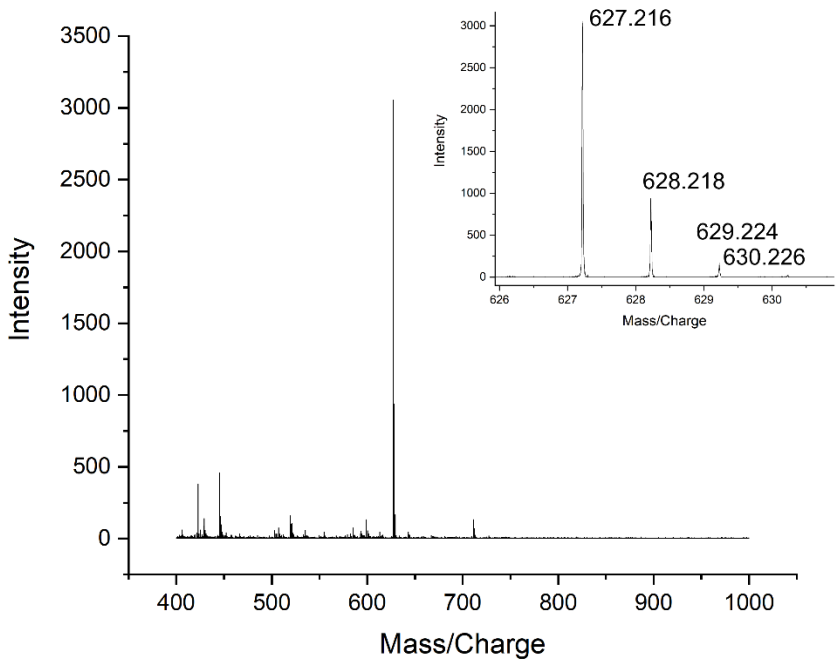


**Figure S10.** High resolution ESI-MS spectrum of **3b**.

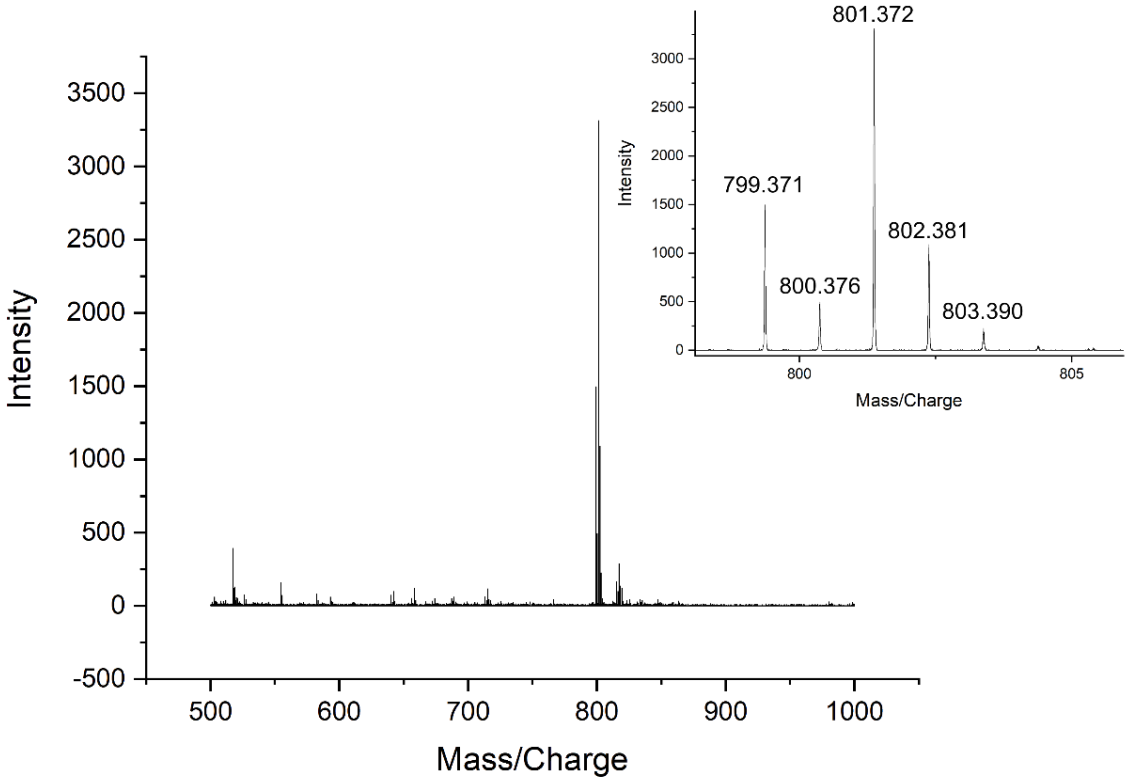


**Figure S11.** High resolution ESI-MS spectrum of **4a**.

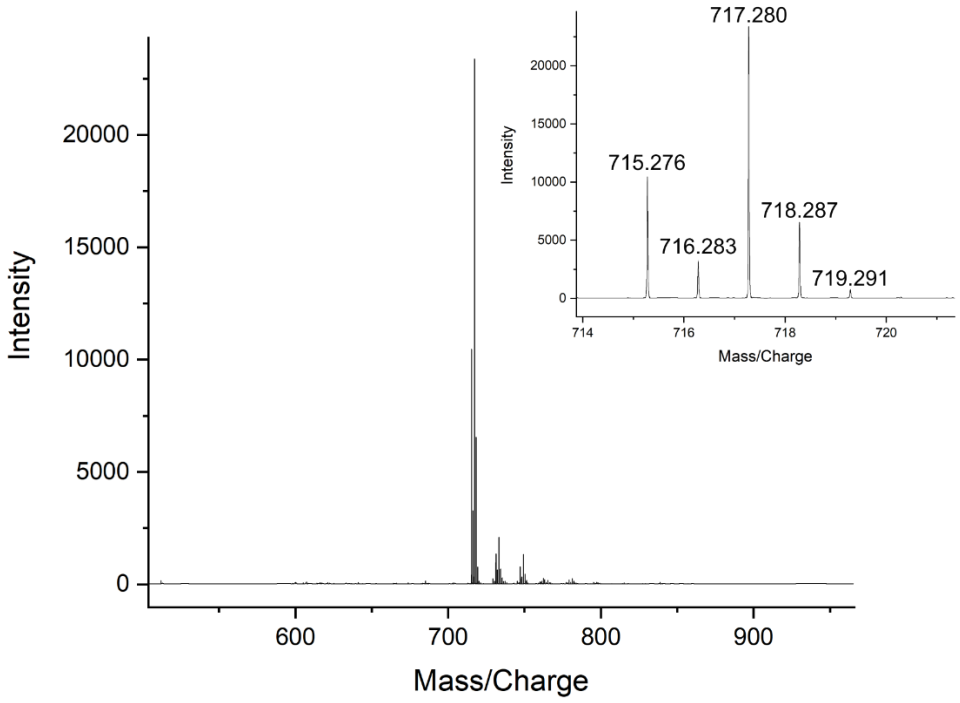


**Figure S12.** High resolution ESI-MS spectrum of **4b**.

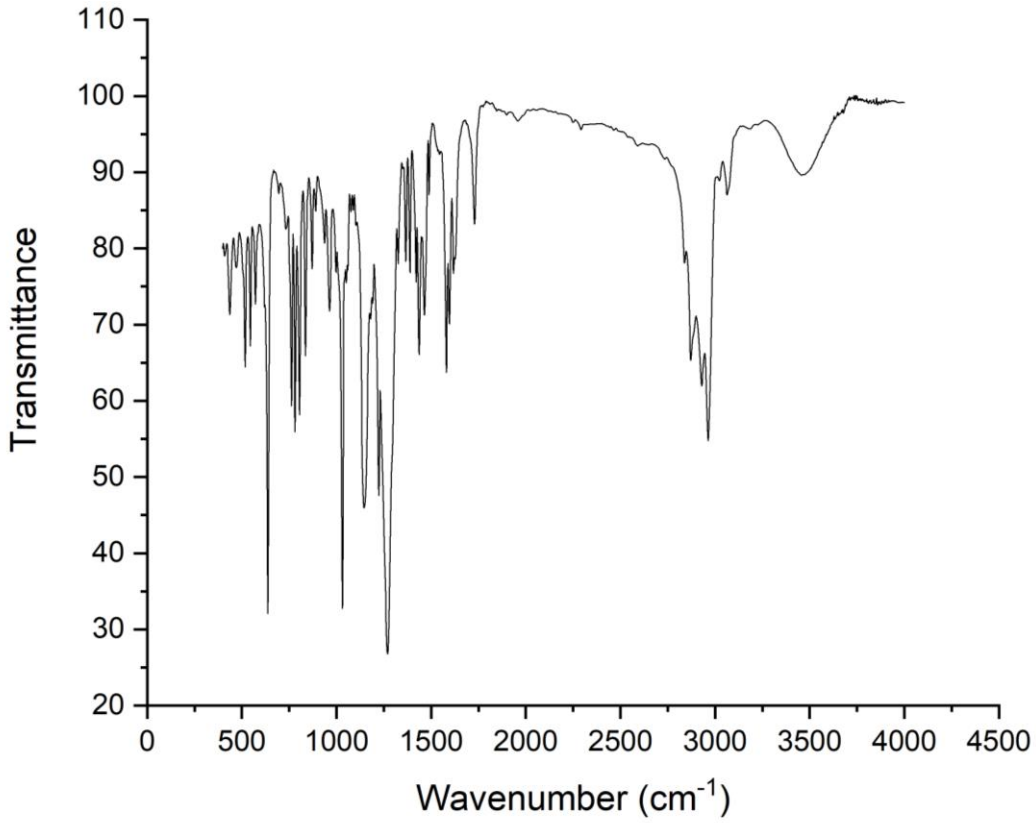


**Figure S13.** FT-IR spectrum of **3a**.

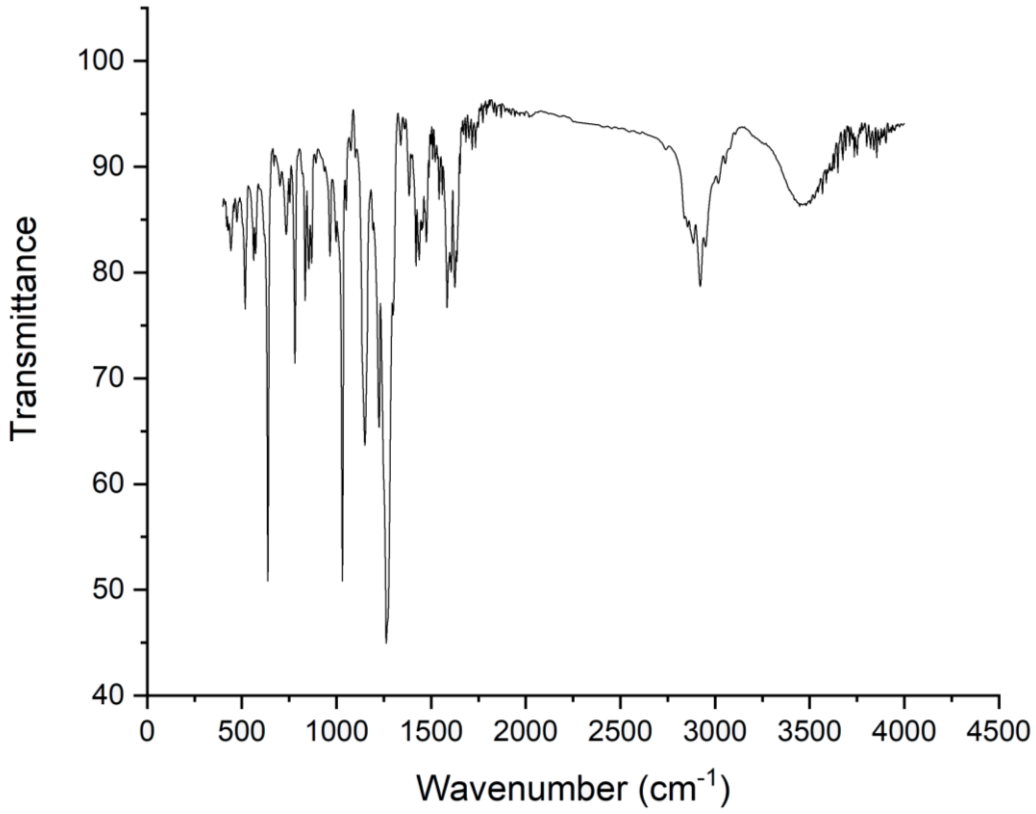


**Figure S14.** FT-IR spectrum of **3b**.

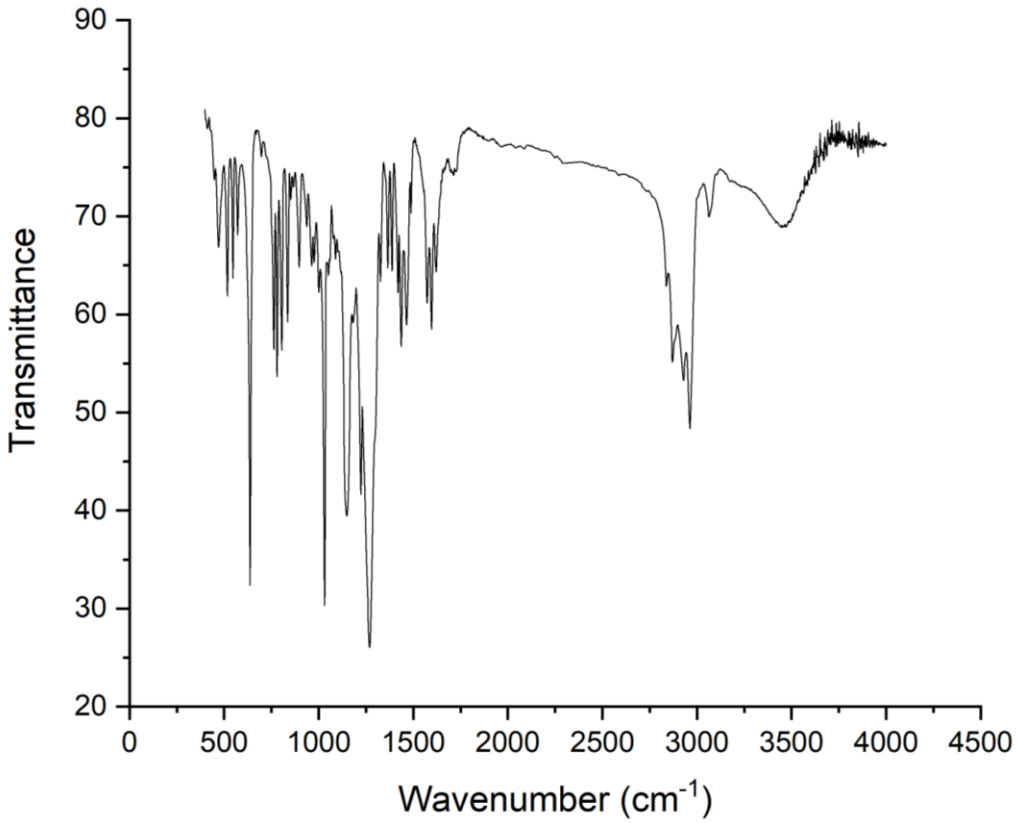


**Figure S15.** FT-IR spectrum of **4a**.

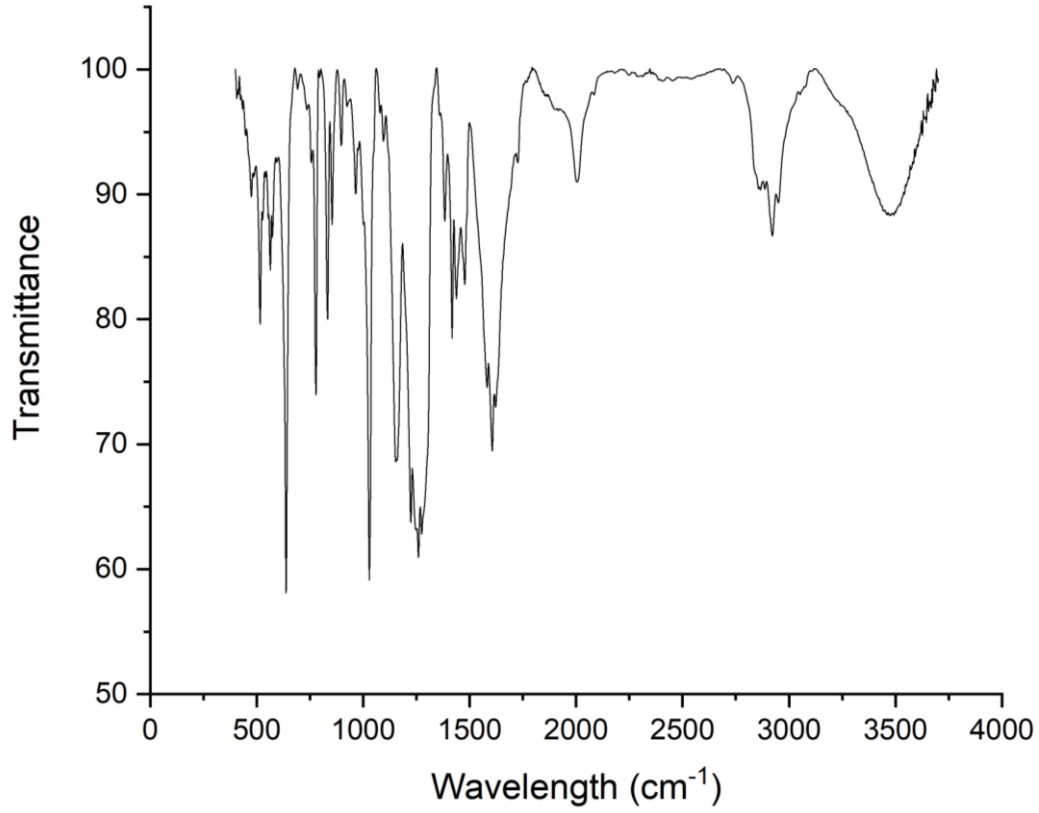


**Figure S16.** FT-IR spectrum of **4b**.

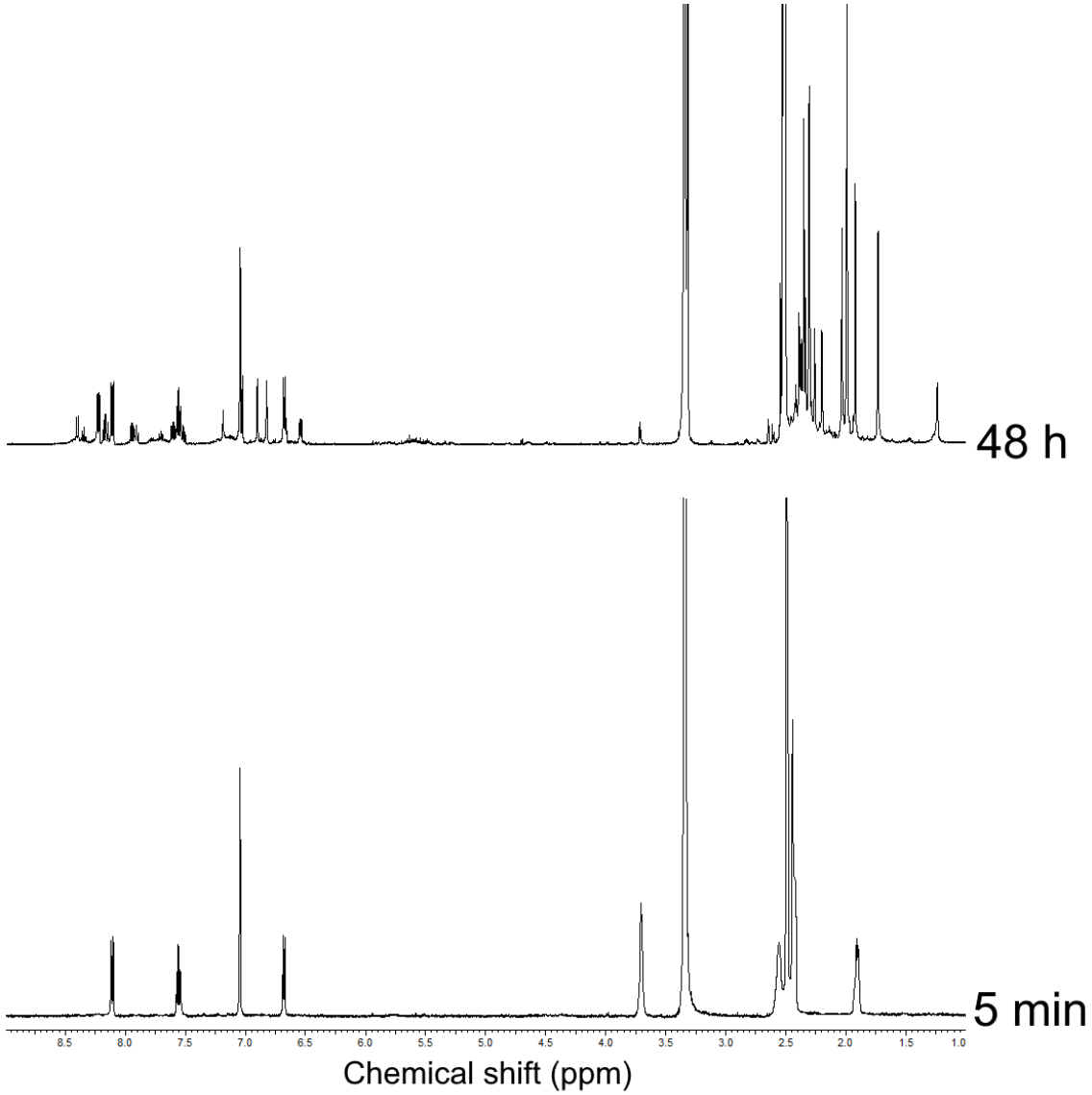


**Figure S17.** Excerpt of $^{1}$H NMR spectrum of **1b** incubated in DMSO-d$^{6}$ for 72 h.

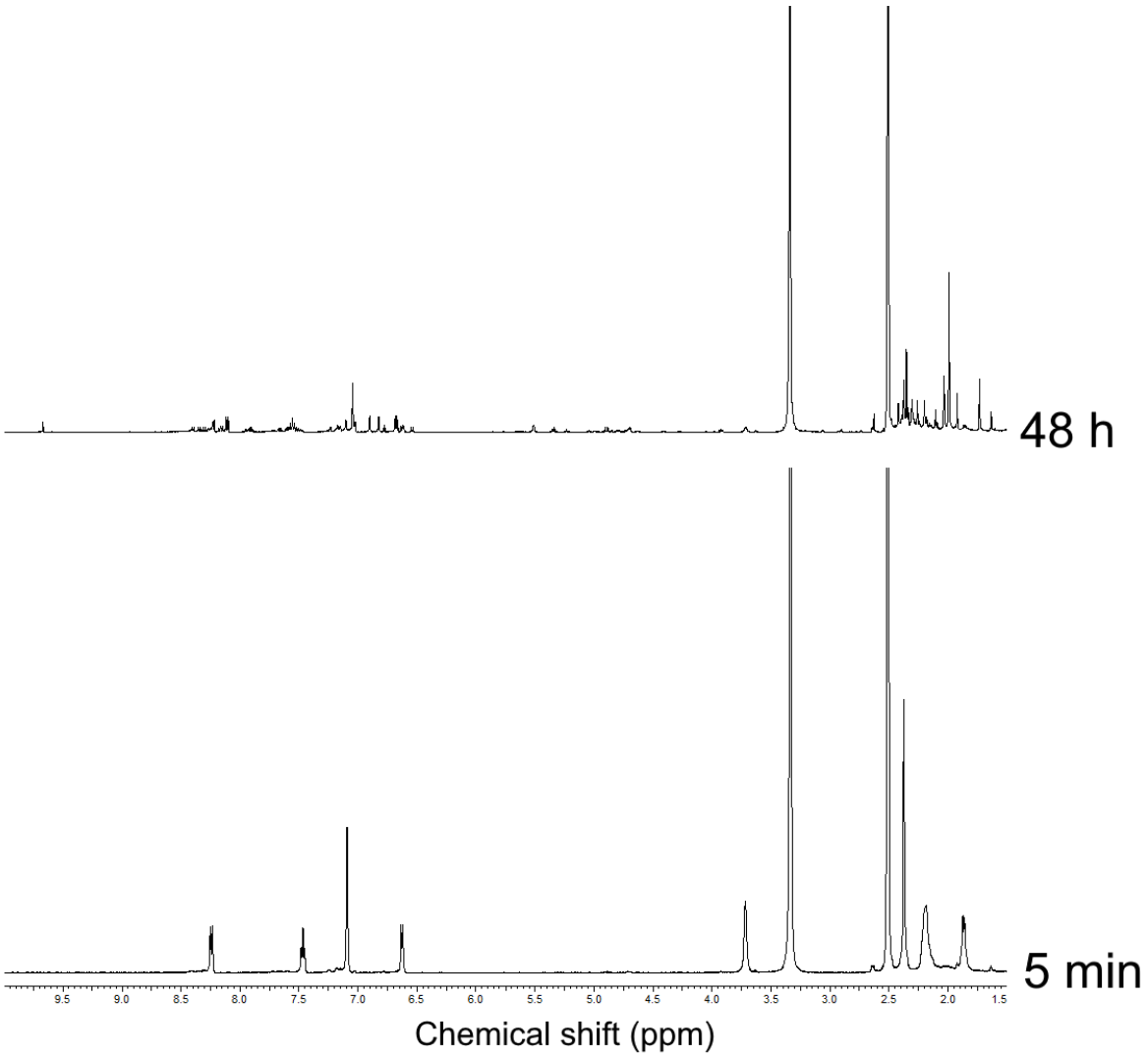


**Figure S18.** Excerpt of $^{1}$H NMR spectrum of **2b** incubated in DMSO-d6 for 72 h.

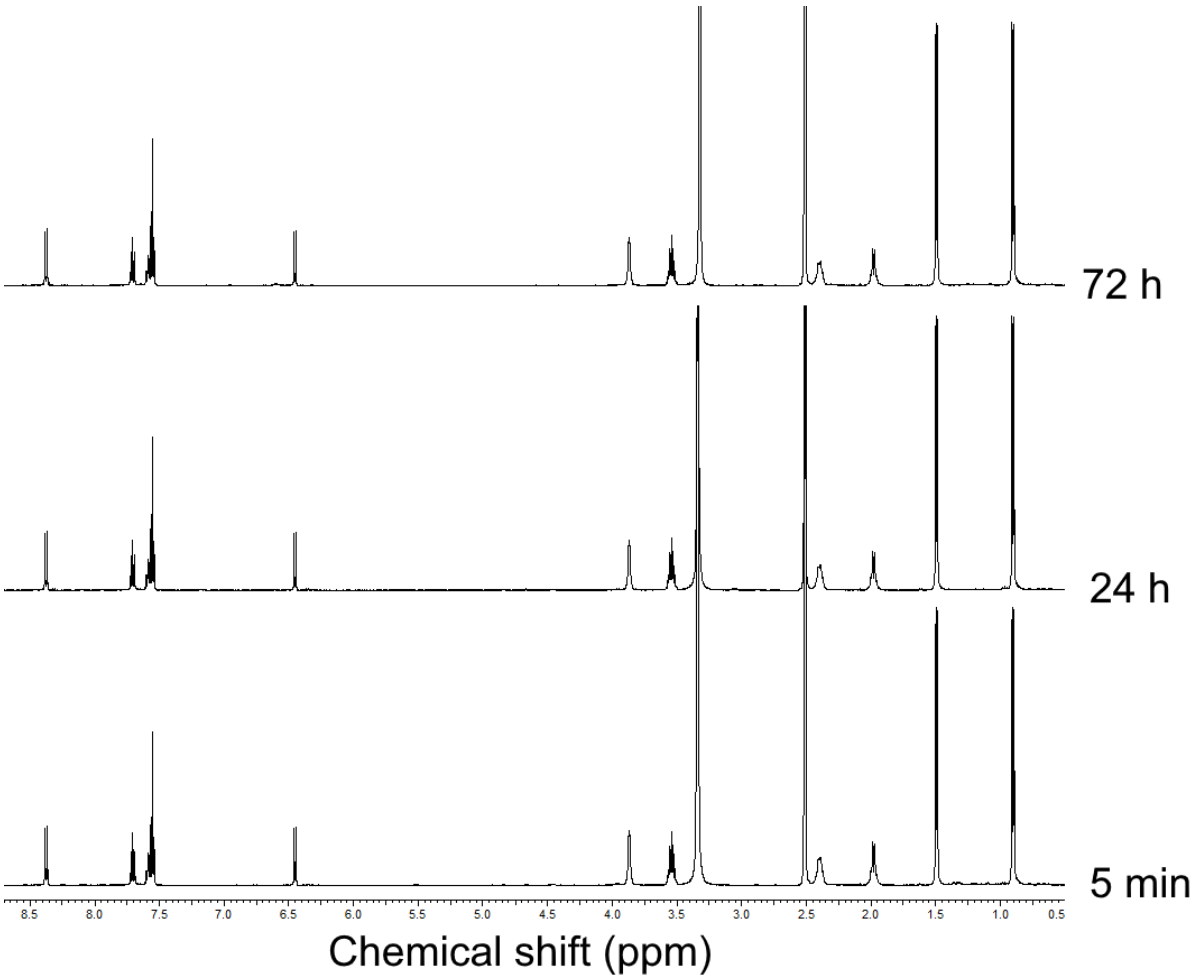


**Figure S19.** Excerpt of $^{1}$H NMR spectrum of **3a** incubated in DMSO-d$^{6}$ for 72 h.

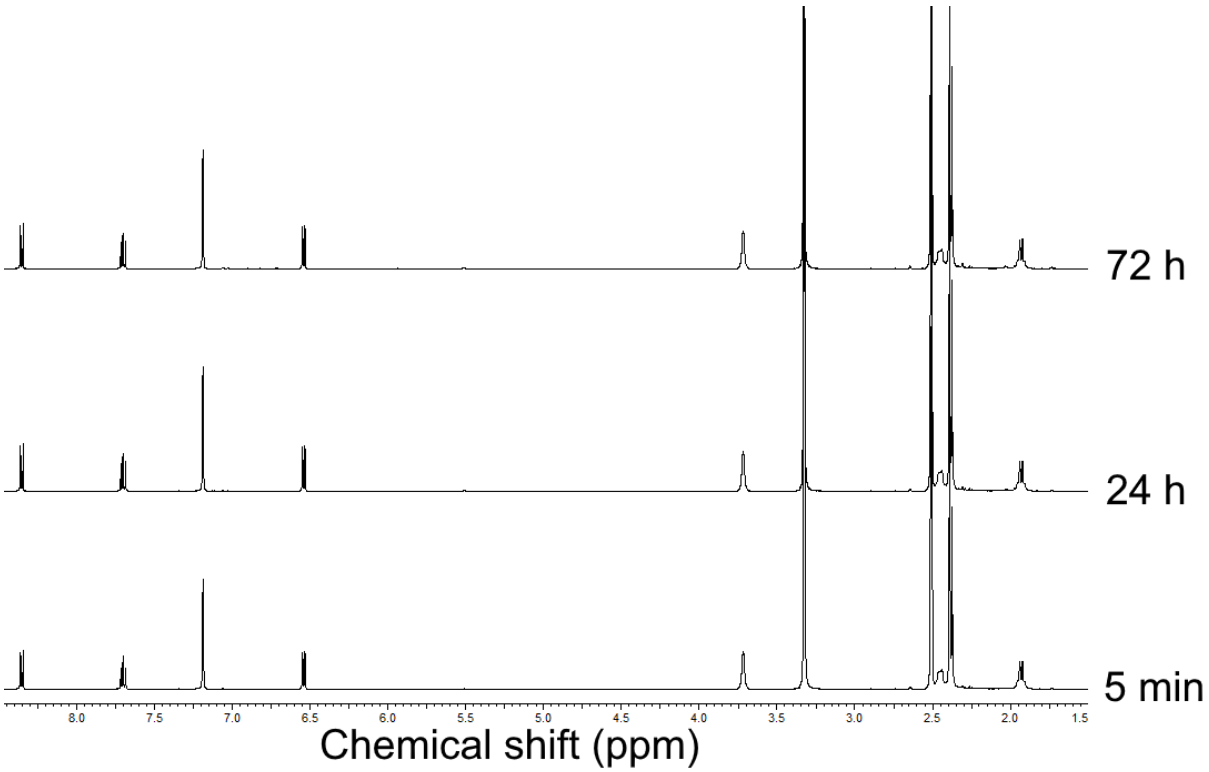


**Figure S20.** Excerpt of $^{1}$H NMR spectrum of **3b** incubated in DMSO-d$^{6}$ for 72 h.

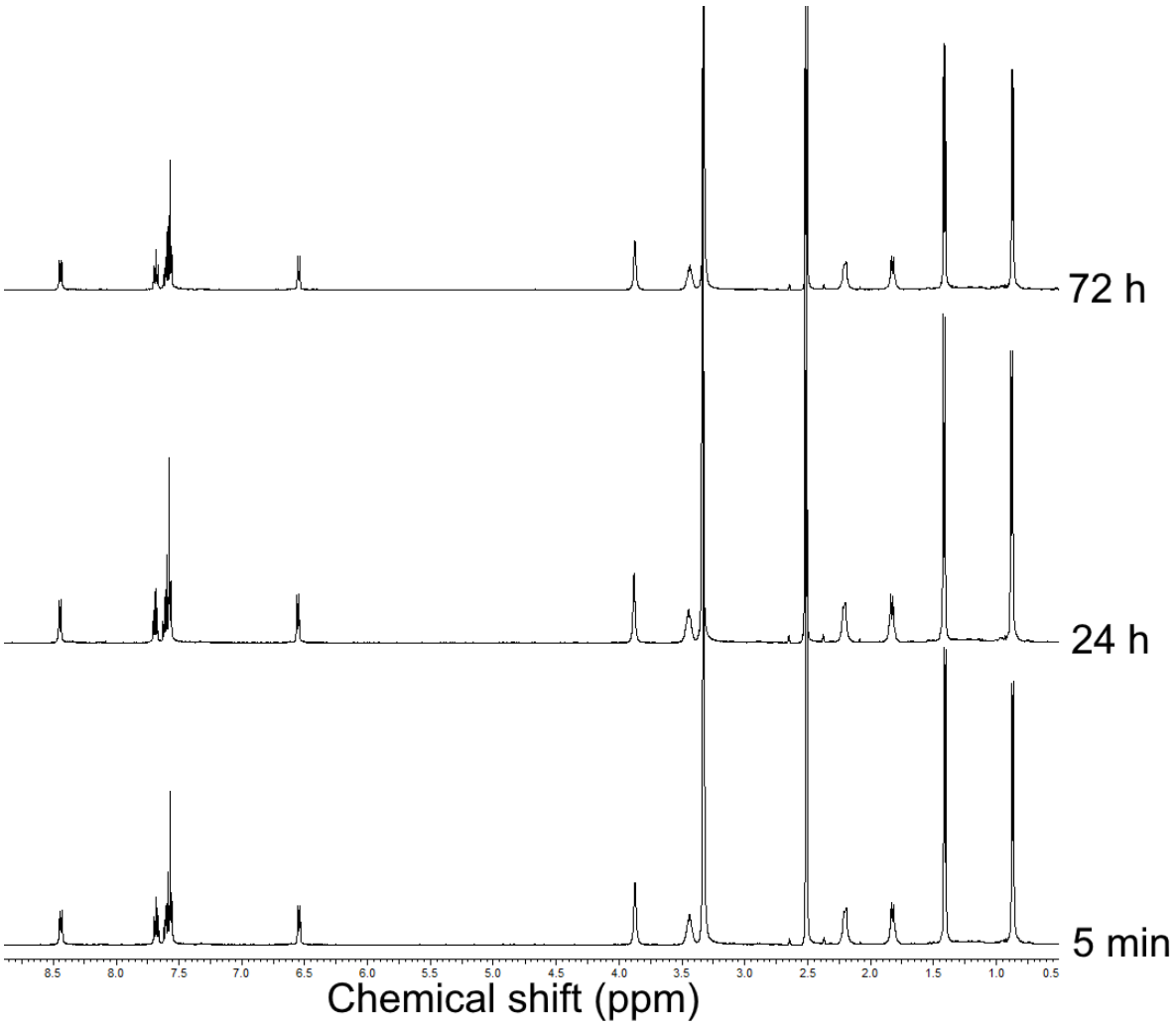


**Figure S21.** Excerpt of $^{1}$H NMR spectrum of **4a** incubated in DMSO-d$^{6}$ for 72 h.

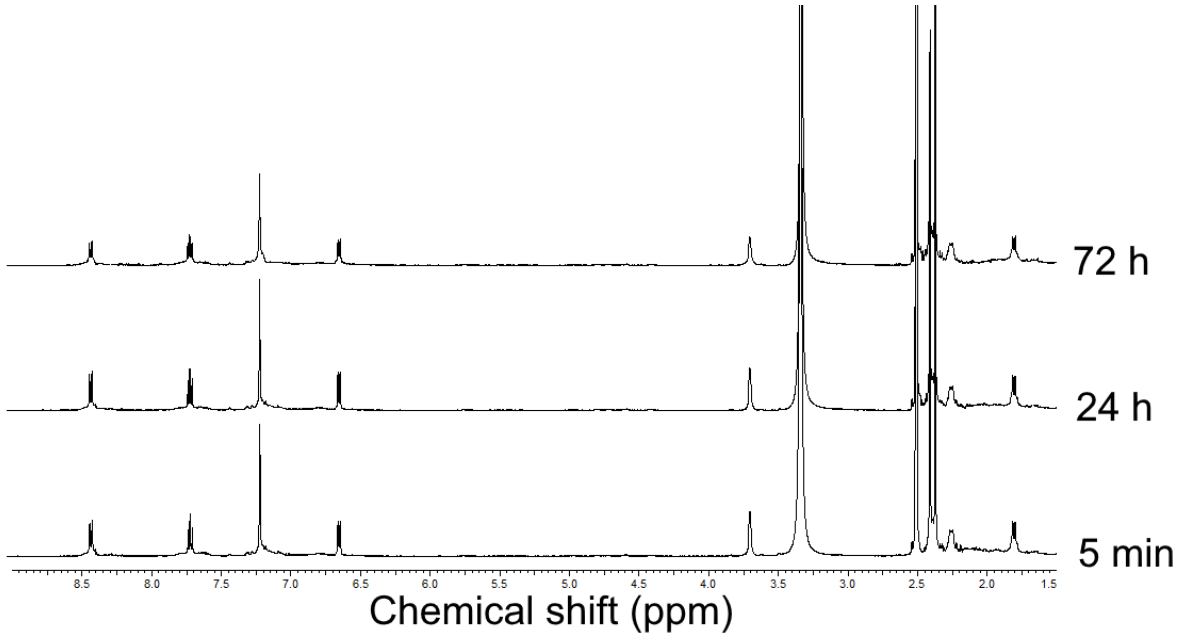


**Figure S22.** Excerpt of $^{1}$H NMR spectrum of **4b** incubated in DMSO-d$^{6}$ for 72 h.

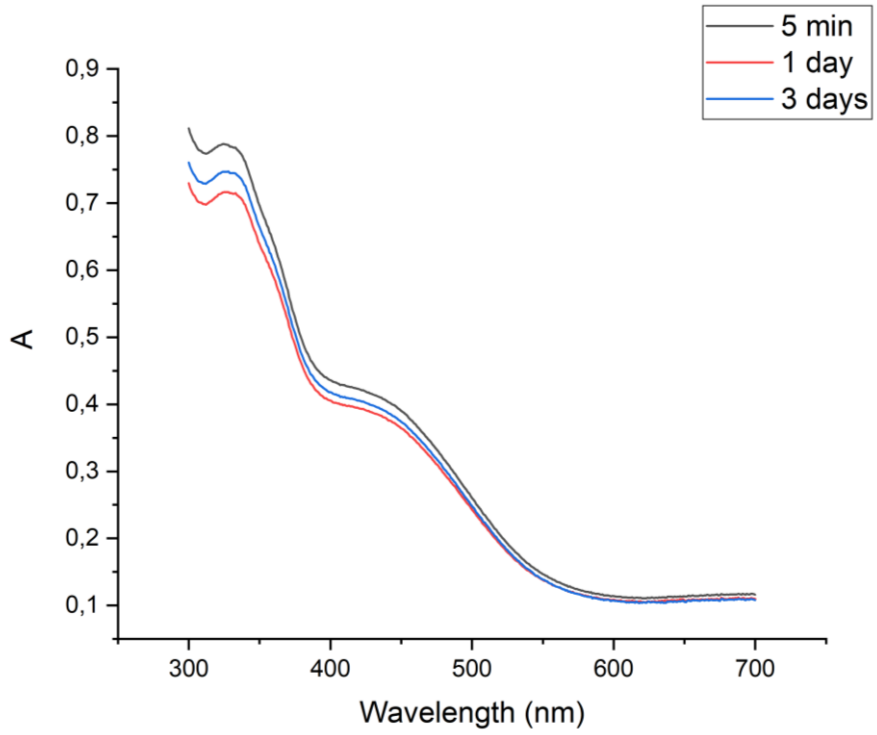


**Figure S23.** Change in UV−vis spectra of **3a** in phosphate-buffered saline (PBS) with 10% fetal bovine serum (FBS) over 72 h.

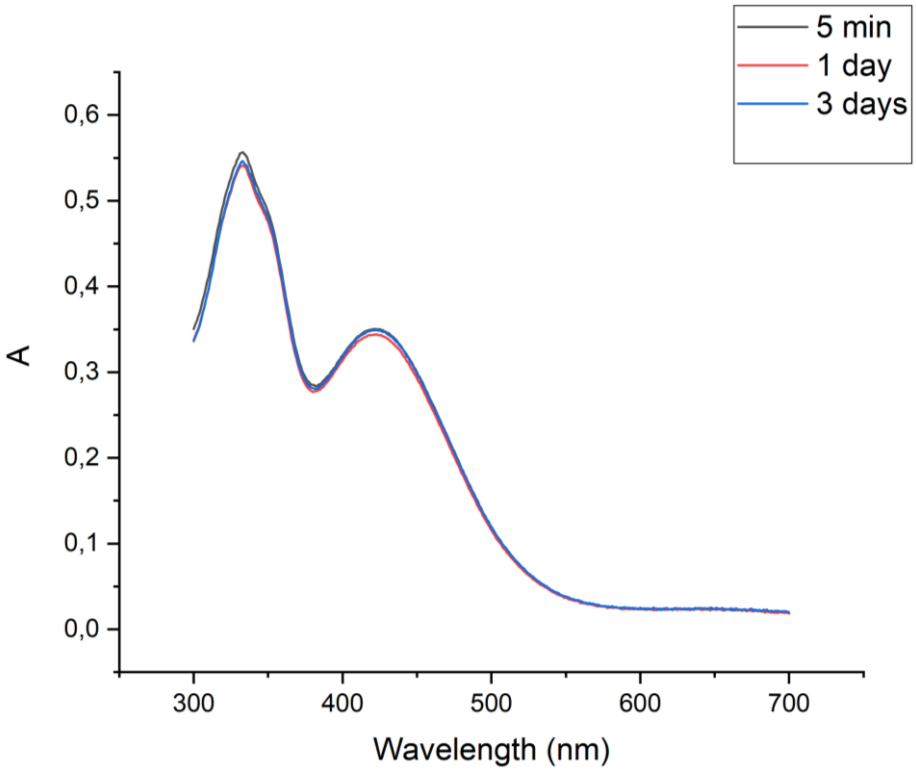


**Figure S24.** Change in UV−vis spectra of **3b** in phosphate-buffered saline (PBS) with 10% fetal bovine serum (FBS) over 72 h.

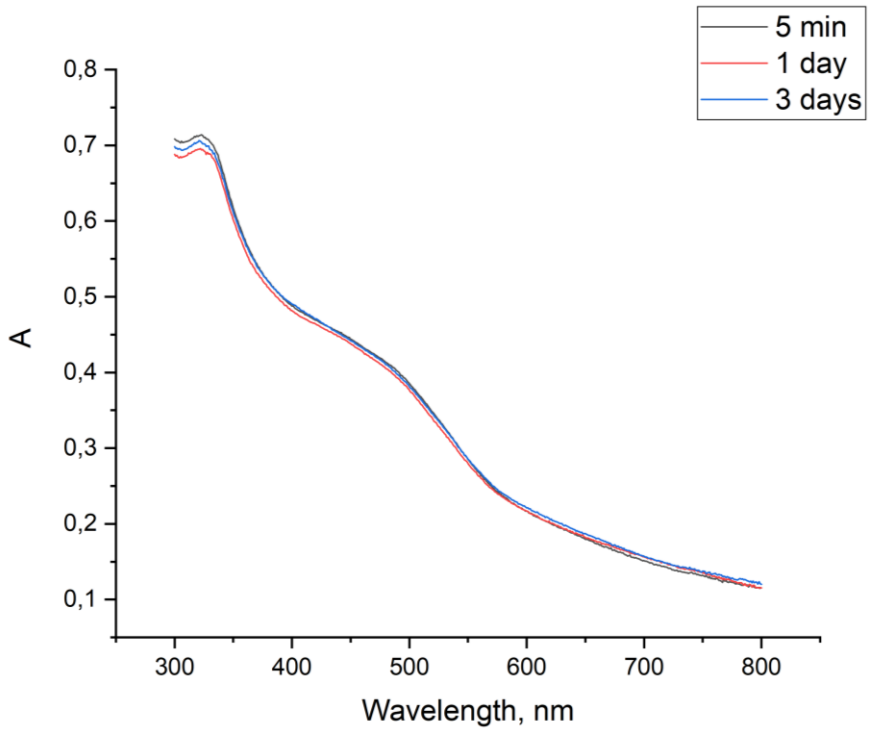


**Figure S25.** Change in UV−vis spectra of **4a** in phosphate-buffered saline (PBS) with 10% fetal bovine serum (FBS) over 72 h.

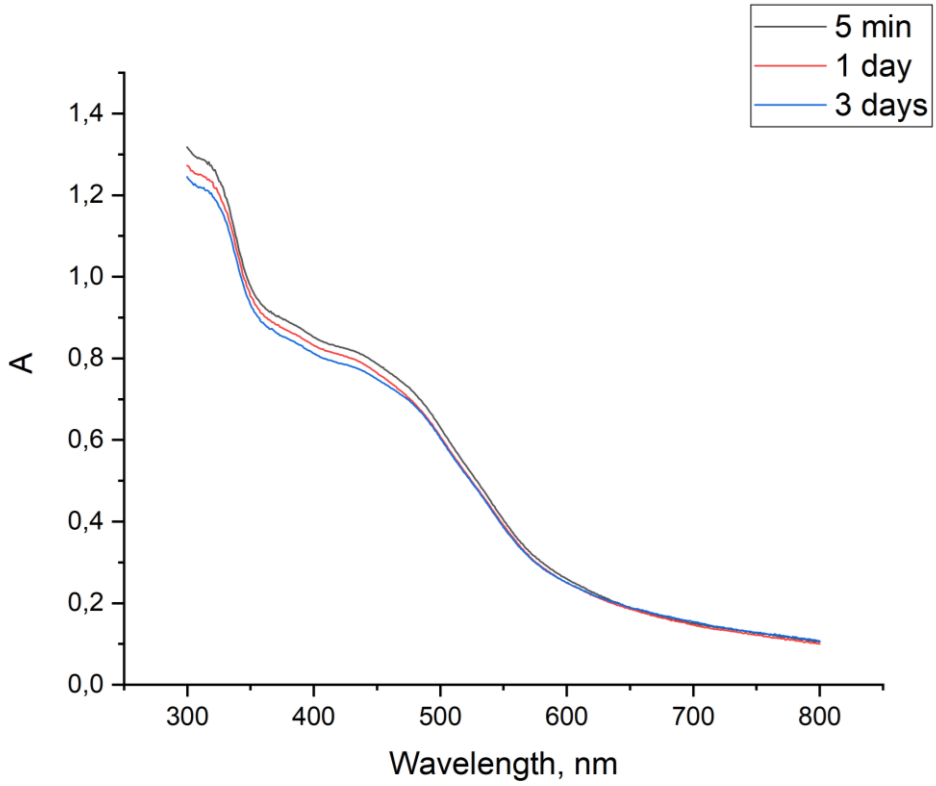


**Figure S26.** Change in UV−vis spectra of **4b** in phosphate-buffered saline (PBS) with 10% fetal bovine serum (FBS) over 72 h.

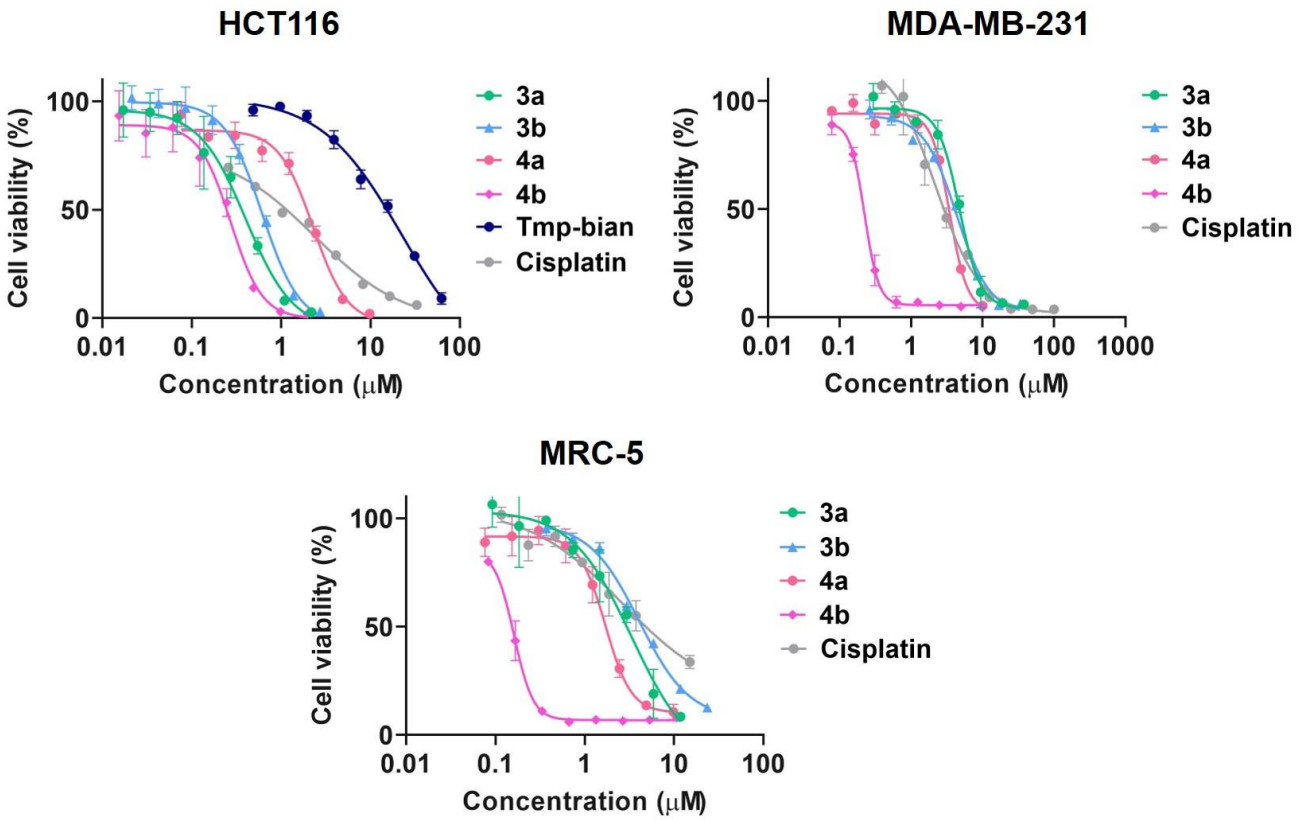


**Figure S27.** Concentration-effect curves of **3a/b** and **4a/b** in HCT116, MDA-MB-231 and MRC-5 cell lines.

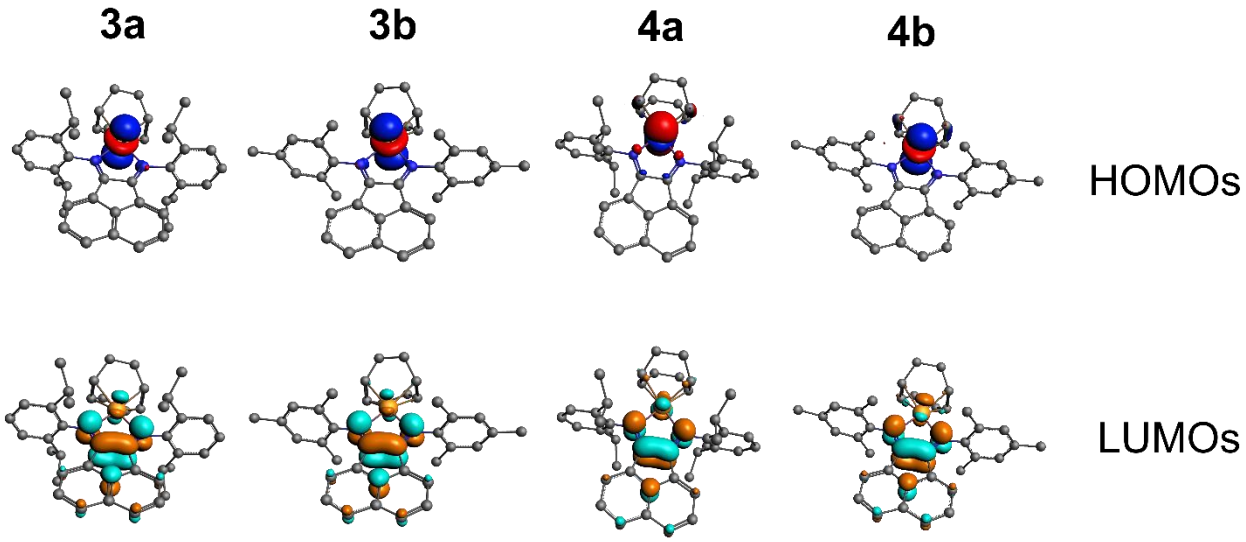


**Figure S28.** Visualization of frontier molecular orbitals in the cations of complexes **3a/b** and **4a/b.** (HOMOs = Highest Occupied Molecular Orbitals, LUMOs = Lowest Unoccupied Molecular Orbitals).

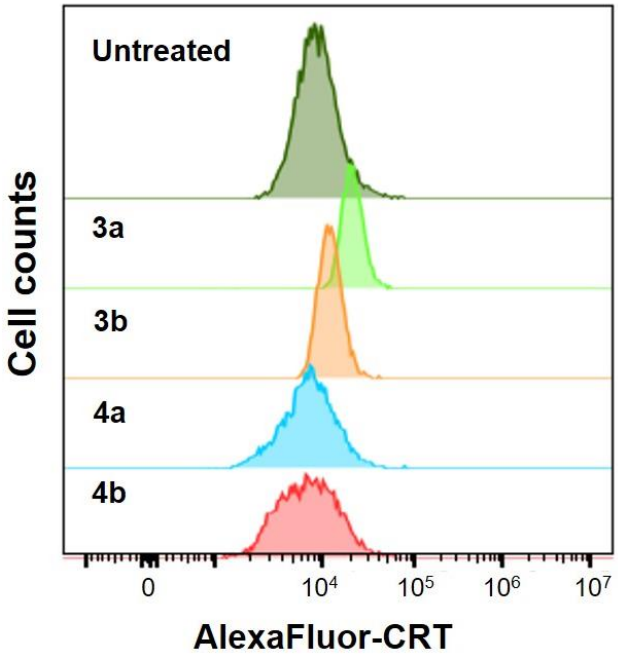


**Figure S29.** Representative flow cytometry histograms, showing the expression of calreticulin (CRT) from PI-negative population of HCT116 cells that were treated with complexes **3a/b** and **4a/b** at equipotent concentrations (10 × $IC_{50\ (72\ h)}$) for 24 h.

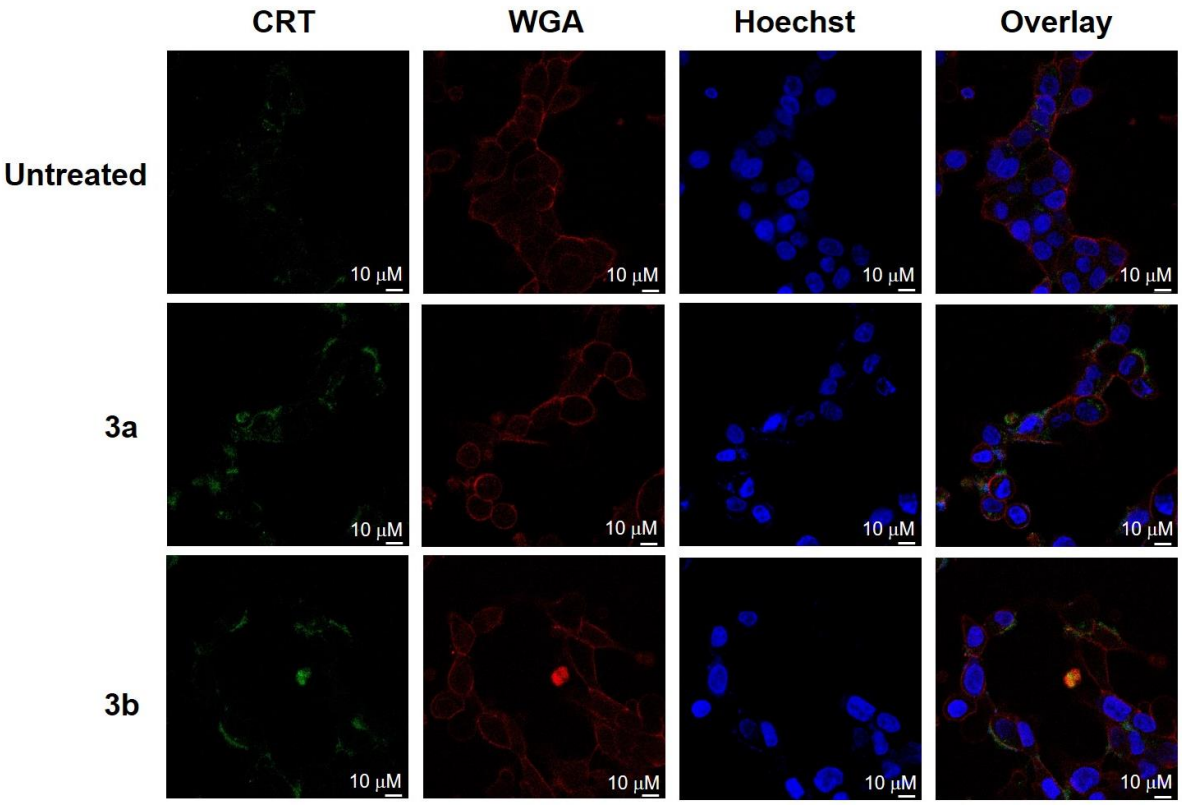


**Figure S30.** Confocal imaging of CRT expression (scale bar 10 μm; Hoechst stains the nucleus, wheat germ agglutinin (WGA) stains the membrane). HCT116 cells that were treated with complexes **3a/b** at equipotent concentrations (10 × $IC_{50\ (72\ h)}$) for 24 h.

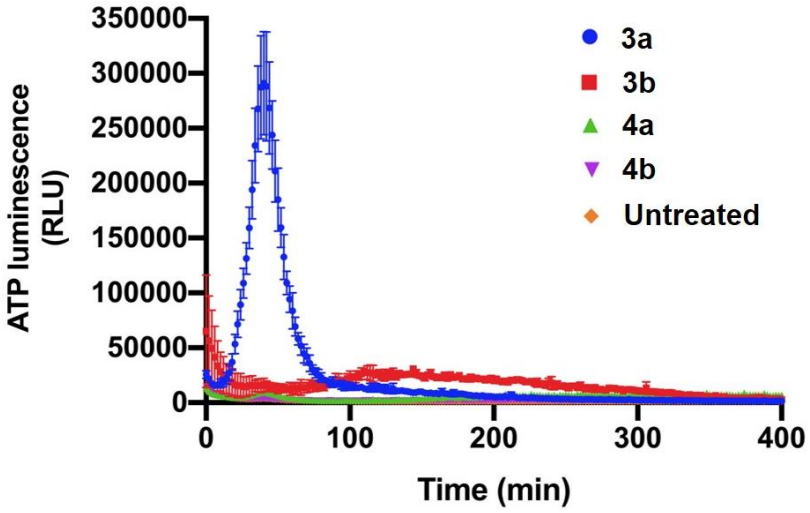


**Figure S31.** Real-time assessment of ATP-dependent luminescence profiles. HCT116 cells were treated with complexes **3a/b** and **4a/b** at equipotent concentrations (10 × $IC_{50\ (72\ h)}$) for 400 min.

## References


1. G. M. Sheldrick, SHELXT–Integrated space-group and crystal-structure determination, *Foundations of Crystallography*, 2015, **71**, 3-8.
2. G. M. Sheldrick, Crystal structure refinement with SHELXL, *Crystal Structure Communications*, 2015, **71**, 3-8.
3. C. B. Hübschle, G. M. Sheldrick and B. Dittrich, ShelXle: a Qt graphical user interface for SHELXL, *Applied Crystallography*, 2011, **44**, 1281-1284.
4. A. L. Spek, PLATON SQUEEZE: a tool for the calculation of the disordered solvent contribution to the calculated structure factors, *Crystal Structure Communications*, 2015, **71**, 9-18.
5. A. Spek, Single-crystal structure validation with the program PLATON, *Applied Crystallography*, 2003, **36**, 7-13.
6. G. t. Te Velde, F. M. Bickelhaupt, E. J. Baerends, C. Fonseca Guerra, S. J. van Gisbergen, J. G. Snijders and T. Ziegler, Chemistry with ADF, *Journal of Computational chemistry*, 2001, **22**, 931-967.
7. J. P. Perdew, K. Burke and M. Ernzerhof, Generalized Gradient Approximation Made Simple, *Physical Review Letters*, 1996, **77**, 3865-3868.
8. E. Caldeweyher, S. Ehlert, A. Hansen, H. Neugebauer, S. Spicher, C. Bannwarth and S. Grimme, A generally applicable atomic-charge dependent London dispersion correction, *The Journal of Chemical Physics*, 2019, **150**, 154122.
9. E. Van Lenthe and E. J. Baerends, Optimized Slater-type basis sets for the elements 1–118, *Journal of Computational Chemistry*, 2003, **24**, 1142-1156.
10. E. v. Lenthe, E. J. Baerends and J. G. Snijders, Relativistic regular two-component Hamiltonians, *The Journal of Chemical Physics*, 1993, **99**, 4597-4610.
11. E. van Lenthe, E. J. Baerends and J. G. Snijders, Relativistic total energy using regular approximations, *The Journal of Chemical Physics*, 1994, **101**, 9783-9792.
12. E. van Lenthe, A. Ehlers and E.-J. Baerends, Geometry optimizations in the zero order regular approximation for relativistic effects, *The Journal of Chemical Physics*, 1999, **110**, 8943-8953.
13. S. Parsons, H. D. Flack and T. Wagner, Use of intensity quotients and differences in absolute structure refinement, *Acta Crystallographica Section B: Structural Science, Crystal Engineering and Materials*, 2013, **69**, 249-259.
14. N. F. Romashev, A. L. Gushchin, I. S. Fomenko, P. A. Abramov, I. V. Mirzaeva, N. B. Kompan'kov, D. B. Kal'nyi and M. N. Sokolov, A new organometallic rhodium(I) complex with dpp-bian ligand: Synthesis, structure and redox behaviour, *Polyhedron*, 2019, **173**, 114110.